

XTE J1859+226: Evolution of spectro-temporal properties, disk-jet connection during 1999 outburst and implications on accretion disk dynamics

Radhika. D^{1,2*}, A. Nandi¹

¹ Space Astronomy Group, ISRO Satellite Centre, HAL Airport Road, Bangalore, 560017, India

² Department of Physics, University of Calicut, Kerala, India

Accepted; Received

ABSTRACT

We investigated the ‘spectro-temporal’ behaviour of the source XTE J1859+226 in X-rays during its outburst phase in 1999, by revisiting the RXTE PCA/HEXTE data in 3 - 150 keV spectral band. Detailed analysis shows that the source evolves through different spectral states during its entire outburst as indicated by the variation in the temporal characteristics (*Quasi-periodic oscillations (QPOs)*, *rms*, *nature of power density spectra (PDS) etc.*) and in the spectral parameters (*disk temperature*, *photon index*, *fold Energy*, *flux etc.*). Evolution of QPO frequencies during rising phase, modeled with propagating oscillatory shock gives an estimate of the oscillating region (*i.e.*, *the Comptonized corona*). Although the evolution pattern of the outburst followed the typical q-shaped profile, we observe an absence of ‘canonical’ soft state and a weak presence of ‘secondary’ emission during the decay phase of the outburst. The broad band spectra, modeled with high energy cutoff, show that fold-energy increases monotonically in the hard and hard-intermediate states followed by a random variation in the soft-intermediate state. These findings make the source evolution more complex. It is also observed that during multiple ejections (observed as radio flares) the QPO frequencies are not present in the power spectra which is dominated by noise component and there is an absence of lag in the soft to hard photons. The disk flux increases along with a decrease in the high energy flux, implying the soft nature of the spectrum. These results are the ‘possible’ indication that the inner part of the disk (*i.e.*, *Comptonized corona*), which could be responsible for the generation of QPO and for the non-thermal Comptonized component of the spectrum, is disrupted and the matter gets evacuated in the form of jet. We attempted to explain the complex behaviour of ‘spectro-temporal’ properties of the source during the entire outburst and the nature of the disk-jet connection before, during and after the ejection events in the context of two different types of accreting flow material, in presence of magnetic field.

Key words: Black holes, Accretion disks, Radiation hydrodynamics, X-ray Sources, Stars: Individual (XTE J1859+226)

1 INTRODUCTION

Galactic Black Hole (BH) sources are interesting objects to study as these sources are observed only in binaries and the process of accretion gets very complex as the disk evolves with time, especially when the sources undergo outbursts and jet ejections take place. Some of the BH binaries show persistent emission (e.g. Cyg X-1) along with aperiodic X-ray variability (e.g. GRS 1915+105), over more than a period of decade. Some BH sources show outbursting behaviour for shorter duration varying from few days to months, and are called as outbursting BH sources or transients (e.g.

GX 339-4, XTE J1118+480, XTE J1748-288, H 1742-322, GRO J1655-40). The outbursting BH sources show different types of intensity variations (*i.e.*, outburst profile) over different period of time (McClintock & Remillard 2006). Some of the sources after being quiescent for a long time, show a sudden increase in the intensity level, and attain a maximum intensity within few days and then decay back slowly to quiescence (H 1743-322, A 0620-00, 4U 1543-47). Their light curves have a ‘Fast Rise and Exponential Decay (FRED)’ profile. Some sources have a slow rise to the peak and decay slowly to the quiescence (GX 339-4, XTE J1752-223) and their light curve profile is termed as ‘Slow Rise Slow Decay (SRSD)’. During this whole phenomena, outbursting sources show different spectral and timing variabilities and exhibit differ-

* E-mail: radhikad.isac@yahoo.in

ent spectral states like *Hard*, *Hard-intermediate*, *Soft-intermediate*, *Soft state* (Homan & Belloni 2005, Belloni 2010) and in some cases a *Very high state* also (Miyamoto et al. 1991, Remilard et al. 1999), in their Hardness-Intensity diagram (HID).

It is also observed that in outbursting BH sources, strong jets are emitted which are seen in radio observations (Fender et al. 2004), during the transition from hard-intermediate to soft-intermediate state in the rising phase (e.g. H1743–322, Miller-Jones et al. 2012) and in the declining phase when the source transits from soft-intermediate to hard state (e.g. XTE J1752–223, Yang et al. 2010). Quasi-simultaneous multiwavelength observations of sources like GX 339–4 (Cadolle Bel et al. 2010), XTE J1748–288 (Brocksopp et al. 2007), H 1743–322 (Miller-Jones et al. 2012), strongly suggests that the radio flares emitted are associated with the disk emission. It has been reported from the study of GRS 1915+105 that, during the jet ejections, QPOs are not observed as well as the Comptonized component gets suppressed (Vadawale et al. 2001). This implies that the inner part of the disk (i.e., ‘hot’ Comptonized corona) gets disrupted and evacuated, and the source spectra softens, suggesting that the X-ray emission is mostly from the disk (Ferozi et al. 1999, Vadawale et al. 2001, Nandi et al. 2001, Chakrabarti et al. 2002, Miller-Jones et al. 2012).

The X-ray transient source XTE J1859+226 was first discovered (Wood et al. 1999) with ASM onboard RXTE (Bradt et al. 1993) on Oct 9, 1999. Subsequently the source was monitored in X-rays with RXTE/PCA and CGRO-BATSE for several months (McCollough & Wilson 1999). The outburst showed the typical FRED profile. Spectral and temporal characteristics confirmed the source as black hole candidate (Markwardt 2001). Several observations in optical and radio wavebands confirmed the presence of the counterpart of the source (Garnavich et al. 1999; Pooley & Hjellming 1999). Spectroscopic studies of the counterpart showed weak emission lines arising from Balmer series of Hydrogen and He II, which is typical for spectra of LMXBs (Wagner et al. 1999). The mass function was estimated to be $(4.5 \pm 0.6) M_{\odot}$, and an assumed inclination angle of 70° gave a lower mass limit of $5.42 M_{\odot}$ (Corral-Santana et al. 2011).

During the 1999 outburst, the source XTE J1859+226 was continuously and extensively monitored in X-rays and in radio, which revealed the X-ray/radio correlations (Brocksopp et al. 2002). The source is observed to exhibit multiple flaring events of five in number. From the study of the spectral evolution in radio, it was found that the jet generation is implied by the production of hard X-rays and also that a correlation exists between soft X-ray and radio ejection during the first flare, while a correlation existed between hard X-ray and radio observation during the other ejections. Casella et al. 2004 studied the temporal properties of the source and found that, the QPOs observed can be classified into three types viz. Type A, B and C. This classification scheme based on the QPO characteristics and phase lag, has been considered as one of the basic formalities to classify the QPOs in Black hole sources (See also Casella et al. 2005; Motta et al. 2011). The phase lag difference between different types of QPOs, suggests that the shape of oscillation is different in different energies. But the evolution of low frequency QPOs (C-type) as well as their origin during the initial rising phase of the outburst is still not clear.

In the context of disk-jet symbiosis of black hole sources, Fender et al. 2004, 2009 have provided a unified picture alongwith the estimation of jet power as a function of X-ray luminosity. Their work also highlighted the occurrence of five Radio flares in XTE J1859+226 and suggested that all the flares occur when the source

is in a similar spectral state. They found that the rms of the PDS reduces during the occurrence of a flare. Rodriguez & Prat 2008 studied the spectral properties of the source during its rising phase and found that the non-thermal flux (2 - 50 keV) remains constant during the first flare of the source. Markwardt 2001 studied the evolution of the source during the rising phase of the outburst and found that there is a signature of partial ‘disappearance’ (absence) of the QPO (or Comptonized corona), when the first radio flare occurred.

Dunn et al. 2011a,b studied the spectral behaviour of this source in the context of global study of disk dominated states of several BH sources. Considering a simple phenomenological model (diskbb+powerlaw) for BH spectral study, Dunn et al. 2011a showed that a large fraction of disk dominated observations of XTE J1859+226 fall below the ‘standard’ Luminosity-Temperature (L-T) relation (see Gierlinski & Done 2004), but the ‘complex’ evolution of hard X-ray spectral nature (cut-off energy, flux etc.) along with the evolution of temporal features (QPOs, rms etc.) are not well explained.

So, in order to have a coherent study of the evolution of temporal and spectral properties of the source (during the entire outburst) as well as the implications on disk dynamics during the multiple ejections, we re-analysed the RXTE PCA/HEXTE temporal and spectral data of the source XTE J1859+226 in the energy band of 3 - 150 keV.

Several models have been proposed to understand the ‘spectro-temporal’ evolution of an outbursting black hole binary. The accretion-ejection instability model (Tagger & Pellat 1999) and global disk oscillation model (Titarchuk & Osherovich 2000) attempts to explain the origin of QPOs. Recently, Ingram & Done 2011 based on propagating mass accretion rate fluctuations in hotter inner disk, and Stiele et al. 2013 based on oscillations from a transition layer in between the disk and hot Comptonised flow have proposed alternative models to explain the origin of QPOs. There have been other attempts also to understand the hard X-ray spectral state variations (Esin et al. 1997; Titarchuk et al. 2007; Motta et al. 2009; Dunn et al. 2011a,b) as well as state transitions across the HID (Meyer et al. 2007; Meyer-Hofmeister et al. 2009) of the outbursting BH sources. But none of these models, as a whole, addressed the issues of evolution of low frequency QPOs as well as soft and hard X-ray spectral components, spectral state changes across the HID during the entire outburst. On the other hand, quite independently, several alternative models (see §4 for discussion) and more recently the phenomenological model (Fender et al. 2004, 2009) have been put forward only for understanding the disk-jet symbiosis in BH sources.

So, we attempted to understand the evolution of temporal and spectral properties associated with the different branches of the ‘q-diagram’ of the outburst of the source XTE J1859+226 within a single framework, which is based on the Two Component Advective Flow (TCAF) model (Chakrabarti & Titarchuk 1995). We also delve deep into the nature of the accretion dynamics during the Jet ejections of this source based on the detailed temporal and spectral X-ray properties.

Similar study (i.e., evolution of ‘q-diagram’) has been performed for GRO J1655–40 (Mandal & Chakrabarti 2010) and GX 339-4 (Nandi et al. 2012) based on this model, whereas the disk-jet symbiosis features observed in GRS 1915+105 are explained in Nandi et al. 2001; Vadawale et al. 2001. Basically, this model consists of two different types of accreting flow (Chakrabarti & Titarchuk 1995): sub-Keplerian (i.e., freely falling and less viscous flow) and Keplerian (i.e., moves in circular orbit and high viscous flow) matter (Shakura & Sunyaev 1973). The

model suggests that the oscillation of the sub-Keplerian shocked-flow (Molteni et al. 1996; Ryu et al. 1997; Chakrabarti et al. 2004; Okuda et al. 2007; Lee et al. 2011), which formed the ‘hot’ Compton corona, could be responsible for the generation of QPOs. In general, outbursting black hole sources show signature of evolution of QPO frequencies (Belloni & Hasinger 1990; Belloni et al. 2005; Debnath et al. 2008; Nandi et al. 2012), which could be explained based on the Propagating oscillatory shocks solution (Chakrabarti et al. 2008, 2009; Nandi et al. 2012) of TCAF model. In this work, we provided the solution of evolution of QPOs during the rising phase and possible explanation of the ‘reverse’ nature of the evolution of the hard spectral component (i.e., the fold energy), which can be interpreted with the shock acceleration mechanism (Chakrabarti & Mandal 2006) in the sub-Keplerian flow. Our findings show that the QPOs are not observed during the radio flares, which we have explained with the possible scenario of ‘evacuation/disruption’ of the inner-part of the disk (i.e., the Comptonized corona). The preliminary results of our findings were presented in Nandi & Radhika 2012.

This paper has been organized in the following manner: In the next section, we discuss the observations and the procedures applied for data analysis using the standard packages for RXTE PCA/HEXTE. In §3, we presented the results obtained from the temporal and spectral analysis for the whole outburst followed by specific details, during each radio flare in §3.2. In §4, we discuss the possible physical scenario to explain the evolution of X-ray properties observed during the entire outburst of XTE J1859+226 and the disk-jet connection, and summarize our conclusions.

2 OBSERVATION AND DATA ANALYSIS

We analysed the public archival data obtained from the HEASARC database for the RXTE satellite to study the nature of the source XTE J1859+226 over the entire duration of the outburst. We analysed the PCA (3 - 25 keV) and HEXTE (20 - 150 keV) data spanning 166 days since October 9, 1999 (MJD 51460.76) to March 23, 2000 (MJD 51626.6). We excluded the observations of July 2000 when the source was in quiescence, as the counts were very less. The standard FTOOLS package of **HEASOFT v 6.11** was used for data reduction. For spectral and temporal analysis purposes, we used the packages **XSPEC v 12.7** and **XRONOS v 5.22** respectively.

For the timing analysis, we used the Science data of PCA in the Binned mode (B_8ms_16A_0_35_H4P, FS37*) of maximum time resolution of 8 ms which spans over 0 - 35 channels, and Event mode (E_16us_16B_36_1s, FS3b*) of 16 μ s time resolution for 36 - 249 channels. We used the FTOOLS task *xfilt* to create filter file, and *maketime* to generate a good time interval (*gti*) file, with conditions of *elevation angle* > 10°, *offset of* < 0.02 and *time since SAA passage* < 30 min. Since it was not possible to select the data only for a single PCU from the Binned mode data, we decided to extract light curves for all PCUs. Light curves were generated in various energy bands of 2 - 6 keV, 6 - 13 keV, 13 - 25 keV and 2 - 25 keV in order to perform an energy dependent study of the PDS. Since the Binned mode data consisted of only 0 - 35 channels (2 - 13 keV), we generated the light curve of minimum binning time, for the channel ranges 0 - 15 (2 - 6 keV) and 15 - 35 (6 - 13 keV), using *saextract*. The light curve from the Event mode data was created using *seextract* for the minimum available binning time, and the data belonging to channel range of 36 - 67 (13 - 25 keV) was extracted from the total available channel range of 36 - 249. A combined light

curve for 2 - 25 keV was obtained, by summing up the light curves from 0 - 35 channels (2 - 13 keV) and 35 - 67 channels (13 - 25 keV), using *lcmath*. Since the contribution of background counts were very less (8.6 counts over 2674 source counts at the peak of the outburst and 6.6 counts over 61.9 source counts at the minimum), we did not subtract the background counts while generating the light curve.

For spectral analysis, we decided to extract data for PCU2 only, since throughout the entire outburst only PCU2 remained ‘ON’ and the efficiency of the detector also holds good. The source spectra were extracted from the Standard2 data product (FS4a*), which has a time resolution of 16 sec. Background spectra was obtained with the help of *runcabackest*, applying the background model for bright source and SAA passage history file obtained from the PCA background web-page¹ of RXTE for the corresponding epoch during which the source has undergone outburst. Spectral response was created using the *pcarsp* tool. We also generated the background subtracted light curve for PCU 2 counts for the energy range 2 - 6 keV, 6 - 20 keV and 2 - 20 keV, in order to plot the HID.

We extracted high energy (20 - 150 keV) spectral data mostly from cluster A (FH52*) of HEXTE, since specific observation by cluster B (FH58*) had lesser counts, except for initial two days (MJD 51462.76 and MJD 51463.83), where there were no cluster A observation. Using standard procedures, we generated the deadtime corrected source and background spectra, and spectral response was generated using *hxtsrp*.

Radio observations were carried out in the bands of 1.43 GHz, 1.66 GHz, 2.25 GHz, 3.9 GHz by various observatories (VLA, MERLIN, GBI, RATAN) during the outburst of the source, and the combined radio light curve was presented in Brocksopp et al. 2002. We re-produced the radio light curve presented in Brocksopp et al. 2002 using the software ‘DEXTER’ (<http://dexter.edpsciences.org/Dexterhelp.html>). Figure 1 shows the X-ray and the radio light curve for the source XTE J1859+226 during the entire outburst.

Brocksopp et al. 2002 (bottom panel of Figure 1) identified five radio flares during the entire outburst. The five flares were observed to have their *peak* radio flux on MJD 51467.90 (F1), 51475.00 (F2), 51479.94 (F3), 51484.62 (F4), 51487.63 (F5).

2.1 Timing analysis

To obtain the PDS from the lightcurves generated, we used the ‘powspec v 1.0’ of the XRONOS package and the customized software based on IDL, *General High energy Aperiodic Timing Software* (GHATS) v 1.0.1². While using ‘powspec’, a normalisation factor of ‘-2’ was applied in order to subtract the expected white noise level from the data, to obtain the squared rms fractional variability from the integral of the PDS. Further analysis shows that the factor of ‘-2’ deviates about 0.5% in almost all states except the soft-intermediate states where it deviates by 3% to 5%. The GHATS package considers dead time effect and hence the correct normalisation factor (as in Zhang et al. 1995) while generating the PDS. The available minimum time binning factor of 0.0078 sec, which corresponds to a Nyquist frequency of 64 Hz was chosen over 8192 segments. The power obtained in the PDS has units of rms^2/Hz .

We modeled the power spectra from 0.1 to 64 Hz, by different

¹ http://heasarc.gsfc.nasa.gov/docs/xte/pca_bkg_epoch.html

² http://www.brera.inaf.it/utenti/belloni/GHATS_Package/Home.html

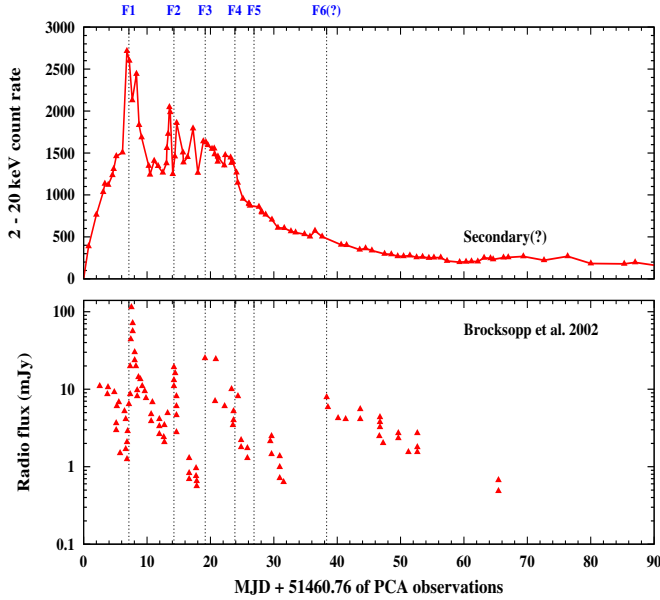


Figure 1. 2 - 20 keV light curve from PCU2 data is shown in the top panel followed by the radio light curve (Brocksopp et al. 2002) in the bottom panel. We also mark the five flares peak as F1, F2, F3, F4, F5. Please see text for flares F5 and F6(?) as there were no radio observation during F5 and before F6.

components of *Lorentzians* (Belloni et al. 2002) for the QPOs and broad-band noise, and a powerlaw for the red noise, wherever required. The resultant centroid frequency for the QPO, is considered as the QPO frequency. We also estimated the Q-factor (centroid frequency/width of the Lorentzian), amplitude in rms and significance of the QPO observed. The standard QDP/PLT command of *stastic* was used to obtain the integrated value (rms) for the QPO and for the overall PDS, in the range of 0.1 to 64 Hz. The error values on each parameter of the components were estimated at 90% confidence interval, using the *fit err* command.

We also studied the evolution of PDS in different branches of HID of the outburst. The phase lag between soft (2 - 6 keV) and hard (6 - 25 keV) photons during the flares was estimated using GHATS. The lightcurves and hence the Fast Fourier Transforms for the 2 - 6 keV and 6 - 25 keV energy bands are generated. The cross spectrum is computed, taking into account the subtraction of Poissonian noise (as per Zhang et al. 1995). We followed the standard procedures of the GHATS package to estimate the lag (see also Casella et al. 2004 & Figure 15 of this work).

2.2 Spectral analysis

We performed a simultaneous fit of the PCA and HEXTE data for the energy range of 3 - 150 keV, including a constant factor of unity for normalising both the spectra. The normalising factor was estimated by simultaneously fitting the Crab spectra during the rising phase of outburst of XTE J1859+226 towards the peak (on MJD 51464.081; Crab observation ID: 40093-01-12-00).

We modeled the energy spectra using the standard accretion disk models (diskbb and powerlaw) for BH spectra, modified by the *phabs* model to account for the interstellar absorption. From an initial fit to the data sets during the entire outburst, we found that the nH parameter has an average value of 0.2×10^{22} atoms cm^{-2} and fixed this value for further analysis. This value of nH , agrees well

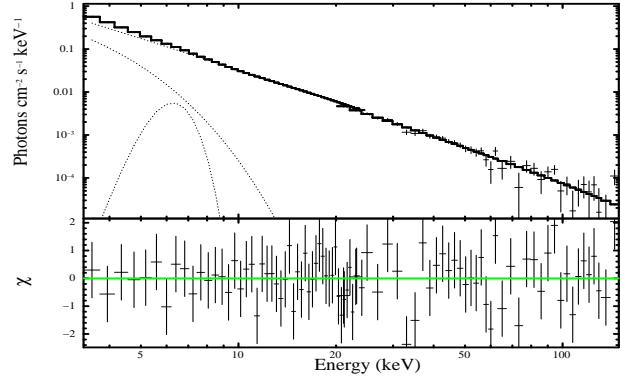


Figure 2. Unfolded PCA (3 - 20 keV) and HEXTE (20 - 150 keV) spectra of the X-ray observation of 24 hrs before the occurrence of first flare (MJD 51466.89, observation ID: 40124-01-11-00). The combined spectra of 3 - 150 keV is modeled by a diskbb ($T_{in} = 0.89$ keV), powerlaw ($\Gamma = 2.35$), a high energy cutoff ($E_{fold} = 151.28$ keV) along with Gaussian & smedge components.

with the average value of 0.216×10^{22} atoms cm^{-2} , estimated by the Leiden/Argentine/Bonn (LAB) survey, and the Dickey & Lockman (DL) survey value of 0.221×10^{22} atoms cm^{-2} (3). Markwardt 2001 quoted a slightly higher value of 1.1×10^{22} atoms cm^{-2} . We find that a change in nH from 0.2 to 1.1, does not significantly change the overall results.

An initial fit, results in residuals around 6.4 keV, which is then modeled by a Gaussian component (*gauss*). The width of the Gaussian was fixed at 0.7 keV. A smeared edge of ~ 8 keV was considered using *smedge* model (Ebisawa et al. 1994). Systematic error of 0.5% was included in all the fits, for considering the uncertainties in the data. We obtained the parameters of disk temperature, disk normalization, photon index with the powerlaw norm and the line energy of the Gaussian line. The photon index of the HEXTE component was tied to that of the PCA component.

For the observation on MJD 51465.49 (observation ID: 40124-01-11-00) during the rising phase of the outburst, a spectral model of *phabs*(diskbb+gauss+smedge*powerlaw)*const* was considered, and the resultant χ^2_{red} ($=\chi^2/\text{dof}$) for the combined PCA-HEXTE fit was 65.81/77. We also attempted to model the spectrum with *compTT* (Titarchuk 1994) to take into account the parameters related to the non-thermal component of the spectra (Comptonized corona), and obtained $\chi^2/\text{dof} = 61.22/88$. Although the fit was statistically good, the variations seen in the parameters were not able to explain the nature of the spectral evolution. We observed that as the source rise towards the peak, the optical depth varied from 1.5 to 0.01, and the seed photon temperature reduced from 2.5 to 0.49 which seems to be unrealistic, although the electron temperature increased from 29 keV to 239 keV. Since the combined spectra showed a cut off in the residuals at higher energies, we decided to include a *highcut* for considering this. The fits improved with $\chi^2/\text{dof} = 58.7/76$. Figure 2 shows the unfolded spectrum for the fits using *highcut* model for one of the observations. Similar method of analysis was followed for all the data sets during the entire outburst.

Since MJD 51486.87 ($\sim 26^{\text{th}}$ day) to the end of the outburst, the HEXTE spectrum was found to be mostly background dominated (few cases spectra upto ~ 50 keV). Hence, we decided to fit only the 3 - 25 keV PCA spectrum using *diskbb*

³ <http://heasarc.nasa.gov/cgi-bin/Tools/w3nh/w3nh.pl>

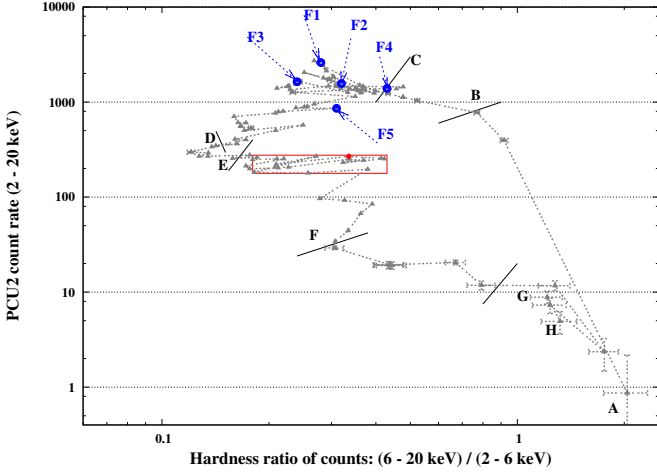


Figure 3. Hardness Intensity Diagram (HID) for the source XTE J1859+226 during the 1999 outburst showing variation of background subtracted count rate with the color, which has been observed with RXTE/PCA (i.e., PCU2). The points marked A \rightarrow H depict the start/state transitions/end of the outburst. The five flares (F1 \rightarrow F5) observed along with the weak signature of secondary outburst phase (marked as rectangular box) are also shown. See text for details.

and *powerlaw*. Better fits were obtained with the model of *phabs(diskbb+gauss+smedge*powerlaw)* with χ^2/dof of 28.62/39 (for observation ID: 40124-01-40-01).

It is to be noted that since we are considering RXTE data ≥ 3 keV only, the value of inner disk temperature obtained from the fits will not be exact. Merloni et al. 2000 pointed out that the diskbb model parameters should not be considered as ideal, since the parameter of disk radius varies due to the change in spectral hardening factor (see also Dunn et al. 2011b).

The convolution model, *cflux* was included to find the flux contribution of the individual components, in the energy range of 3 - 150 keV. The error values for each parameter were obtained using the *err* command at a confidence interval of 90%. We observe that the uncertainty in flux estimated using *cflux*, is not of large variation, except a few cases of the soft-intermediate state where a 5% variation is observed. The variation between the values obtained by *cflux* and *flux* commands are found to be a maximum of 4%.

3 RESULTS

In this section, we present the nature of the HID along with variation of X-ray and Radio flux. In Figure 1, we show the intensity variations of the emission from the source, both in X-rays and radio. We observe that as the source rises from quiescence, the background subtracted X-ray Count rate (2 - 20 keV) rises from ~ 1 count/sec (MJD 51460.76 = 0th day) to a peak of 2714 counts/sec (MJD 51467.58). Previous studies carried out by Homan & Belloni 2005 and Casella et al. 2004 also show that for the first observation, the count rate is ~ 1 . But it is to be noted that the error on the count rate is very large (see Figure 3). The radio flux peaks (MJD 51467.9) at a value of 114 mJy resulting in peak flare F1, implying the release of matter in the form of jets (Brocksopp et al. 2002). The radio flux then reduces and peaks at 19 mJy (MJD 51475) resulting in 2nd flare (F2), almost after 7 days of the peak flare F1. We observe that the X-ray intensity also reduces, and peaks again with 2045 counts/sec (on MJD 51474.28). A third peak radio flare (F3)

is observed of flux 31 mJy (on MJD 51479.9), after a gap of 4 days from the previous flare (F2), with the increased X-ray intensity of 1637 counts/sec.

The next flare (F4) has a peak flux of 5.2 mJy (on MJD 51484.6), where the X-ray intensity is around 1391 counts/sec. The source count rate starts decreasing from 1444 counts/sec (after MJD 51483.94) to ~ 4.9 counts/sec (MJD 51626.6 = 166th day) and attains quiescence. While decaying, the source is observed to show a weak secondary emission (see §3.1.5) for around 24 days with peak emission on 69th day (MJD 51530.13) of the outburst. A fifth flare (F5) is reported by Brocksopp et al. 2002 based on ASM lightcurve to occur on MJD 51487.6, but there were no radio observations on that day. F5 occurred during the declining phase of the outburst with X-ray intensity ~ 870 counts/sec.

Figure 3 shows the HID (see also Homan & Belloni 2005; Dunn et al. 2011a) plotted using the background subtracted PCU2 count rate. The points where the five flares occurred are also marked in the Figure (see also Fender et al. 2009). The possible transitions which occurred, are labelled from A to H. In general, outbursting sources undergo state transitions from *hard* \rightarrow *hard-intermediate* \rightarrow *soft-intermediate* \rightarrow *soft* \rightarrow *soft-intermediate* \rightarrow *hard-intermediate* \rightarrow *hard* (Homan & Belloni 2005; Belloni et al. 2005; Belloni 2010; Nandi et al. 2012) and finally into a quiescent state. In Figure 3, point A corresponds to the first PCA observation (MJD 51460.76 = 0th day). Although on this day, the source count rate is very less (~ 1 counts/sec) with large error bars, this observation is important to follow the evolution of the source since the beginning of the outburst. As mentioned earlier similar value of count rate was quoted by Casella et al. 2004 and Homan & Belloni 2005. From point A to B, the source remained in the initial hard state where there is an increase in soft photons but the spectra remains hard as indicated by the hardness ratio. From B to C, the source remained in the hard-intermediate state. After C, the source moved to the soft-intermediate state (CD). We found that flare F1 has taken place during the transition of hard-intermediate to soft-intermediate state, and all the flares which have occurred are associated with the branch CD. In the soft-intermediate state (See also Fender et al. 2009), the hardness ratio is comparatively lesser than AB and BC, implying the softening of the spectra. The source seems to have occupied a soft state DE (which is not ‘canonical’, see §3.1.4) for a very short duration and then continued in the soft-intermediate state itself during the declining phase of the outburst in the branch EF. The source then, transits from soft-intermediate (EF) to hard-intermediate state (FG). Very few observations have been obtained during this phase. Finally, the source enters into hard state (declining phase) and subsequently reaches quiescence (after H).

The outburst profile and hardness-intensity variation shows a weak signature of secondary emission (see §3.1.5 for details) of the outburst, which is marked as rectangular box in Figure 3. The weak presence of soft state (see §3.1.4) and the weak ‘secondary’ emission (see §3.1.5), makes the HID different from the ‘standard’ evolution pattern of other outbursting sources (Homan & Belloni 2005; Belloni et al. 2005; Belloni 2010; Mandal & Chakrabarti 2010; Nandi et al. 2012).

In the following sub-sections, we will present the evolution of temporal and spectral properties (in broad spectral band of 3 - 150 keV) associated with different branches of HID of the source XTE J1859+226 to understand the accretion dynamics from a theoretical point of view. We will also describe the X-ray features during the Radio flares to investigate the disk-jet symbiosis. The results

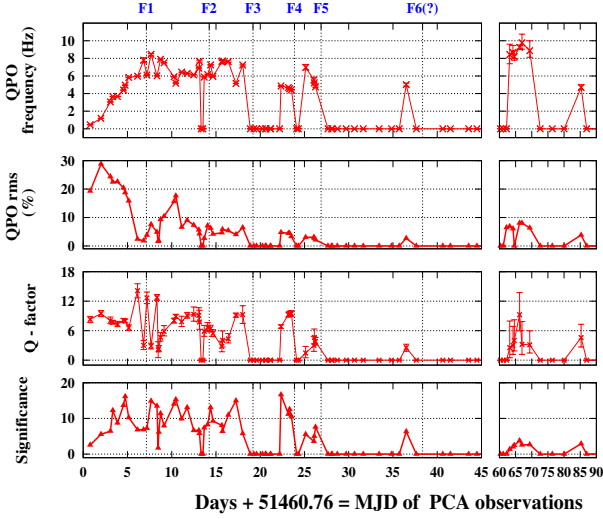


Figure 4. Evolution of QPO frequency, QPO-rms, Q-factor and significance throughout the outburst of XTE J1859+226. ‘Disappearance’ of QPOs during radio flares (ejections) are shown in the plot. Radio flares peak timings (in unit of days) are also marked as F1, F2, F3, F4 & F5 (see Table 2 for details).

are examined in the light of two different type of accreting flow materials and explained in the discussion.

3.1 Temporal & Spectral evolution

In Figure 4, we show the variation of QPO frequency, QPO rms, the Q-factor and significance of the QPO observed, over the entire outburst of the source XTE J1859+226. The QPO frequencies increase monotonically from 0.46 Hz to 6.09 Hz in the rising phase of the outburst, which is a quite natural phenomena as observed in other outbursting BH sources (Belloni & Hasinger 1990; Belloni et al. 2005; Nandi et al. 2012). In the later phase of the outburst, the presence/absence of QPO frequencies are directly linked with Jet emission (see Figure 4, §3.2) as well as with the ‘secondary’ emission of the outburst (see Figure 1, §3.1.5).

The evolution of QPO frequencies during rising phase can be understood based on the Propagating Oscillatory Shock (POS) solution (Chakrabarti et al. 2008, 2009; Nandi et al. 2012) of the TCAF. According to this model, the oscillating frequencies observed as QPOs are due to the movement of the shock surface (i.e., Comptonizing region). The POS solution states that the QPO frequency is inversely proportional to the infall time scale and the QPO frequency (ν_{QPO}) can be obtained with a knowledge of the instantaneous shock location or vice-versa, and the value of the compression ratio ($R = \rho_+/\rho_-$, where ρ_+ and ρ_- are the densities in post and pre shock flows). According to Ryu et al. 1997, Chakrabarti & Manickam 2000, the frequency of the shock location is similar to the observed QPO frequency. Thus, the QPO frequency for an axisymmetric toroidal bounded system (i.e., shock surface; see Figure 17) can be written as $\nu_{QPO} = \nu_{s0}/t_{infall} = \nu_{s0}/[2\pi R r_s (r_s - 1)^{1/2}]$, where $\nu_{s0} = c/r_g$ is the inverse of the light crossing time of the BH, and $r_g = 2GM/c^2$ for a BH of mass M . Since the shock will be drifting with time (Chakrabarti et al. 2008, 2009), the time dependent shock location can be expressed as $r_s(t) = r_{s0} \pm v_0 t/r_g$, where r_{s0} is the shock location at time $t=0$ and v_0 is the corresponding shock velocity (Chakrabarti & Manickam 2000; Molteni et al. 1996). The ‘+’ sign is used for an outgoing

shock in the declining phase and the ‘-’ sign is used for an infalling shock during the rising phase. In Figure 5, we show the evolution of QPO frequency with time (days) during rising phase of XTE J1859+226, which we modeled using above equations of the POS solution. Fitted result allows to calculate the shock location and hence to estimate the size of the Comptonizing region. Similar attempts have been performed for GRO J1655–40, XTE J1550–564 (Chakrabarti et al. 2008, 2009), GX339–4 (Nandi et al. 2012) and H1743–322 (Debnath et al. 2013).

The first day of PCA observation is considered as $t=0$ sec. Figure 5 shows that the initial three observations of QPO follows one trend while the rest shows another. Hence the evolution follows two different solutions for different parameters (shock location, velocity etc.). The FWHM obtained from the fits to the Lorentzian feature of the QPO has been considered as error bars. The fit to the initial three QPO frequencies gives the value of compression ratio as $R=5$, initial shock location r_{s0} of $105.1 r_g$ ($t=0$ sec) and the shock velocity $v_{s0} = 6.8 \text{ ms}^{-1}$. The fit to the rest of the QPO frequencies during the rising phase gives $R=3.8$, $r_{s0}=48.8 r_g$, $v_{s0}=1.4 \text{ ms}^{-1}$. The overall fit yields a mass of BH of $\sim 8M_\odot$ (mass estimate is consistent as reported by Dunn et al. 2011b) with reduced χ^2 of 1.046. In the final fitting, we excluded the last observation (as shown in cyan color) on MJD 51466.89, which is just before the first radio flare (F1). The variation of shock locations (i.e. the size of Comptonising region) is shown in the same Figure (circle-dotted line in dark). The oscillation of shock stalled at $21.2 r_g$ and gives the estimate of minimum size of the comptonizing region (before the F1 flare). From Figure 5, it can be observed that there is a kink (see also Chakrabarti et al. 2009; 1998 outburst of XTE J1550–564) at the point where the two fitted functions meet. It is possible that at the kink the disk dynamics has changed suddenly. This could be implied by the variation in the different spectral parameters observed, as mentioned in §3.1.2.

Evolution of the parameters of the spectral fit, obtained from the analysis are shown in Figures 6, 7 and 8. Figure 9 depicts the variation of disk flux and powerlaw flux in the 3 - 20 keV range and also for the 20 - 150 keV powerlaw flux; and Figure 10 shows the fraction of thermal flux contributing to the total 3 - 20 keV flux, the contribution of thermal flux over non-thermal flux (3 - 20 keV) and also that of the flux ratio in 3 - 20 keV to 20 - 150 keV energy range (upto MJD 51486.82).

3.1.1 Hard state (branch AB)

During the first PCA observation (point A in Figure 3), the PDS was dominated by broad-band noise only. The next observation (on MJD 51461.54) has a red noise along with a prominent QPO of 0.45 Hz (not reported by Casella et al. 2004), which is marked as the first point in the top panel of Figure 4 and Figure 5. We observe that the QPO frequency starts rising from 0.45 Hz to 1.19 Hz (type C QPOs; see Casella et al. 2004 for details), with the rms amplitude increasing from 19.2 to 28.8 (Figure 4). Also, we find that in the AB branch, the power spectra is mostly dominated by red noise along with QPO, and the rms of PDS varies from 30% to 24%. This variation in total rms is similar to that observed in other BH sources like GX 339–4 (See Munoz-Darias et al. 2010). In this branch, we found that as the source flux rises from quiescence, the photon index of the energy spectra rises from 1.6 to 2.0, the disk temperature (T_{in}) varies in-between 1.01 keV to 0.83 keV (Figure 6) and hard X-ray flux dominates over the disk flux (Figure 9). The variations observed in this branch are typical of low/hard spectral state. At the same time, the hard X-ray spectral component (i.e., fold energy) increased from 53 keV to 114 keV.

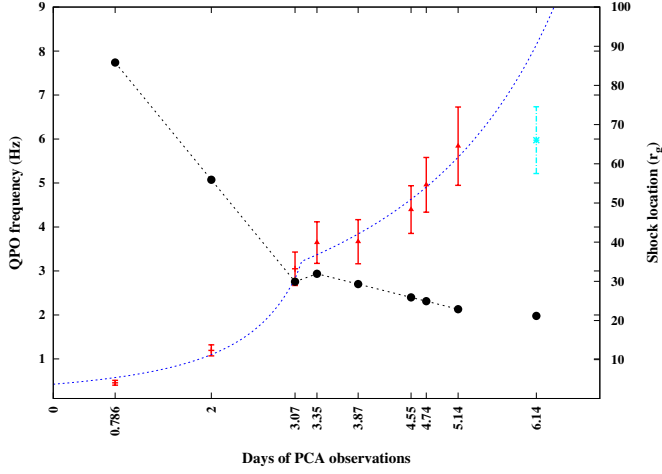


Figure 5. Evolution of QPO frequency with days, during the rising phase of the outburst of XTE J1859+226. The FWHM of the fitted Lorentzian of the QPO has been considered as the error bars. The curves show the fitted solution based on the POS model. The dark circles and the associated line (second y-axis) show the variation of the shock location (i.e., Comptonizing region; See also §4 for discussions on the same).

3.1.2 Hard-intermediate state (branch BC)

In the hard-intermediate state (BC), we find that the power spectra has a flat top noise along with QPOs and a powerlaw form at frequencies > 10 Hz, with the total rms varying from 24% to 16% and the QPO frequency increasing from 3.05 Hz to 5.97 Hz (Type C; see Casella et al. 2004). The fundamental QPO frequency is observed along with sub-harmonic frequencies before and after the fundamental, with the ratio among all being 1:2:4. The photon index increases from 2.0 to 2.4 and the disk temperature slowly increases from 0.75 keV to 0.85 keV. The disk flux is increasing as compared to the non-thermal powerlaw flux in the energy band of 3 - 20 keV (Figure 9), as well as the contribution of low energy to high energy powerlaw flux increases (Figure 10).

A kink around 3rd day (see Figure 5) in rising phase, when the QPO frequency changes from 3.05 Hz to 3.64 Hz, is peculiar in sense that there is an abrupt change in the photon index from 2.05 to 2.2 along with an increase in disk flux from 0.42×10^{-9} ergs $\text{cm}^{-2} \text{s}^{-1}$ to 0.7×10^{-9} ergs $\text{cm}^{-2} \text{s}^{-1}$. It could be possible due to sudden change in the accretion flow dynamics during this phase.

Figure 7 shows that during branch BC, the fold energy increased from 108.3 keV to 201.2 keV. Thus we observe an increase in fold Energy from 53 keV to 201.2 keV, when the source moves through the branches AB and BC during the rising phase. Earlier studies performed on the sources GX 339-4 and XTE J1550-564 by Motta et al. 2009 and Titarchuk & Shaposhnikov 2010 respectively, shows that the non-thermal component (cut-off energy/fold Energy) decreases when the source moves through the hard and hard-intermediate states, during the rising phase of the outburst. This seems to suggest that the nature of monotonic increase of fold Energy seen in rising phase is different from that observed in other BH sources (See Figure 6 of Motta et al. 2009, and Figures 1 and 2 of Titarchuk & Shaposhnikov 2010). The ‘reverse’ evolution of the fold energy seems to be unnatural, and hence a different physical mechanism could be involved for the generation of non-thermal component (see §4 for discussion).

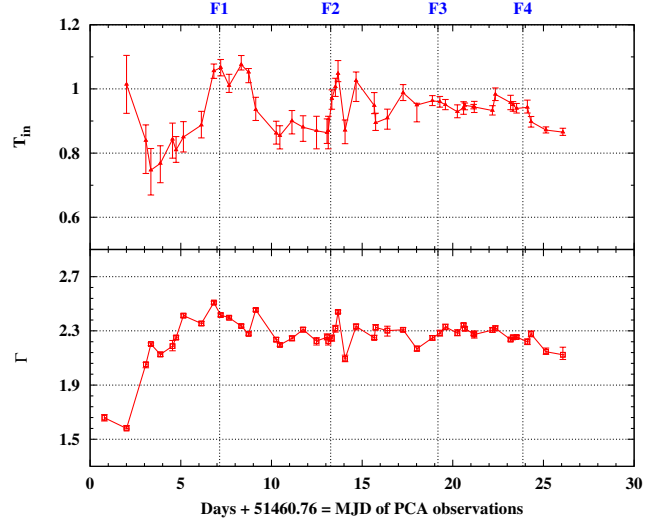


Figure 6. Evolution of the spectral parameters, disk temperature (T_{in}) and photon index (Γ) of observations before flare 5 (F5) of the source XTE J1859+226.

3.1.3 Soft-intermediate state (branch CD)

During the initial phase of the branch CD (from MJD 51468.4 to MJD 51473.82), the steepness of the red noise component starts decreasing and the power spectra has a flat top noise along with QPOs (both A and B types). Further observations of QPOs for the next 9 days, has been classified into type C by Casella et al. 2004. For two observations on MJD 51474.42 and 51475.42, type B QPOs are present, which are classified as *Cathedral or twin QPOs*. QPOs observed after MJD 51483.117 (for > 1 day) are of type B, while those after MJD 51484.276 are not classified into any types (Casella et al. 2004). Initially, the QPO rms increased upto 18% and gradually decreased to $\sim 5\%$, whereas Q-factor varies in between 3 to 12, randomly. The total rms of the PDS is observed to increase from 7% to 14%. During the end phase of the branch, after MJD 51484.87, the PDS has only broadband noise of amplitude 6% to 3% rms, with or without QPOs along with a power-law form from 10 Hz to 64 Hz.

The photon index varies around 2.5 to 2.1, and the disk temperature from 1.07 keV to 0.85 keV, suggesting that the source remain in the soft-intermediate state. The fold energy is observed to vary randomly in between 64 keV and 180 keV, around an average of 130 keV within 1σ error bars (except few data points, which are within 1σ to 2σ). The disk flux is seen to vary randomly, whereas the power-law flux decreases gradually as shown in Figure 9. During the later phase of this state, the disk temperature slightly decreases from 0.85 keV to 0.7 keV and photon index decreases from 2.4 to 2.0 (Figure 8).

The variations in the temporal & spectral parameters suggest that this branch CD has the characteristics of soft-intermediate state. During this state, multiple ejection events have occurred and observed in Radio as flares (Brocksopp et al. 2002). Fender et al. 2009 has reported on the features of HID and temporal characteristics during a flare. We present a detailed observational results of the spectral and temporal properties, during each of these flares in §3.2.

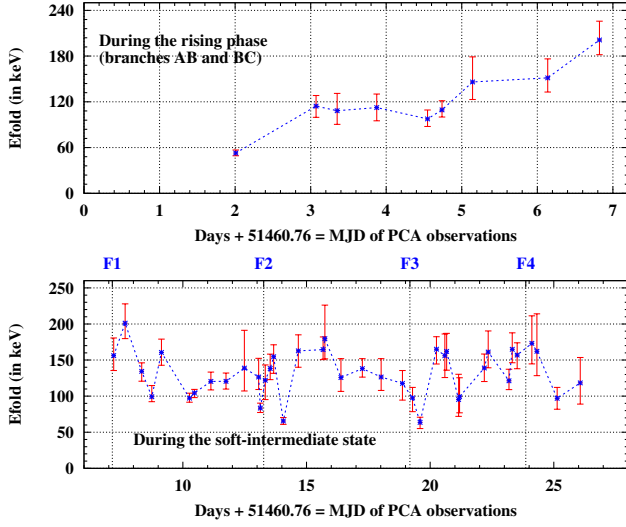


Figure 7. Evolution of fold Energy (E_{fold}) during the rising phase (branches AB, BC; top panel) and soft-intermediate state (branch CD; bottom panel) of the HID for the source XTE J1859+226.

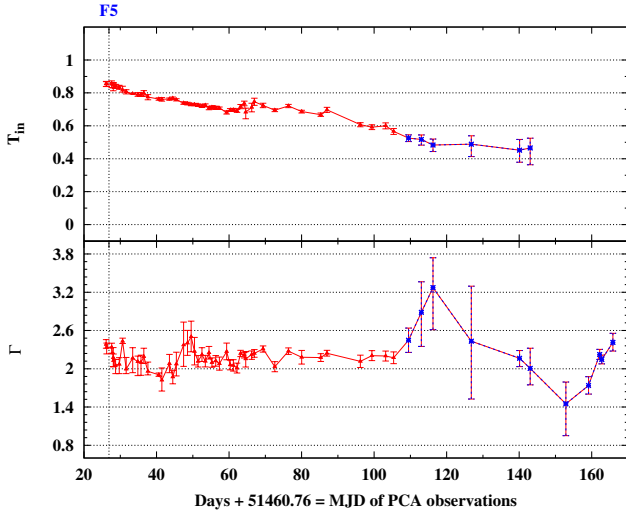


Figure 8. Evolution of the spectral parameters (3 - 25 keV energy range), disk temperature T_{in} , photon index Γ for observations from flare 5 (F5) till the end of the outburst of XTE J1859+226. Note, spectral data is fitted upto 15 keV (around 120th day) during the unusual variation of photon index.

3.1.4 Soft-state (branch DE)

During the transition from branch CD, we find that a few of the observations (MJD 51504.31 to MJD 51510.29 in Figure 1) show hardness ratio around 0.1 (Figure 3) and total rms $\sim 1\%$ to 2% , which suggest a short presence of soft state (see Munoz-Darias et al. 2010). Similar value of hardness ratio was quoted in Figure 19 of Casella et al. 2004, Figure 1 of Homan & Belloni 2005 and Figure A.1 of Dunn et al. 2011a, for this source. During these observations the thermal flux dominates (see top panel of Figure 10) the spectra and QPOs are also absent. But the other spectral features during this phase seem not to imply the characteristics of the ‘canonical’ soft state as suggested by McClintock & Remillard 2006. We observe that as compared to branch CD (soft-intermediate state), the disk tempera-

ture reduces from 0.9 keV to 0.7 keV (*to be noted that it is not the exact value, due to the limitations of RXTE and diskbb model (Merloni et al. 2000)*) and the photon index remains ~ 2.2 (spectra are harder compare to soft-intermediate state). These variations seen are very different from the observations of other BH sources where the disk temperature remains high above 1 keV, photon index is >2.5 during the soft state (See §4.3.5 and Figures 4.8 and 4.9 in McClintock & Remillard 2006; Belloni et al. 2006). All these findings deviate from the ‘canonical’ description of soft spectral state observed in outbursting BH sources (Belloni et al. 2005, 2006; McClintock & Remillard 2006; Belloni 2010).

3.1.5 Soft-intermediate state (branch EF)

In branch EF, no significant QPOs are observed (Casella et al. 2004 has not classified the QPOs also), and the PDS has broadband noise of rms value $\sim 3\%$. We observe that the disk temperature decreases (from 0.7 keV to 0.5 keV) and the photon index varies at ~ 2.2 as similar to branch CD. The source is in the declining phase and we observe that the disk and power-law flux starts gradually decreasing (Figure 9) without any signature of hard X-ray flux beyond 50 keV.

- The outburst profile (top panel of Figure 1, see also Figure 3) indicates that, during this phase there is an enhancement in X-ray flux and it gradually decreases to the quiescence. This increase in flux has also been observed by ASM on-board RXTE. From the spectral analysis, we observed that there is an increase in the disk and powerlaw flux (Figure 9) along with increase in disk temperature (Figure 8) for ~ 24 days (i.e., from 63rd to 87th day of the outburst; see also Figure 1). Although the value of inner disk temperature (T_{in}) is less, we note that the variation in uncertainty of T_{in} is less than the value of T_{in} itself (McClintock & Remillard 2006). But as mentioned in §2.2 and §3.1.4, we do have to consider the constraints in the diskbb model and energy range considered. The increase in disk and powerlaw flux can also be noted in Figure 14 of Dunn et al. 2011a, after \sim MJD 51530. Although such an increase in flux has been observed in other sources like GX 339–4 (Dunn et al. 2011a), but the observation (\sim MJD 52710) was associated with hard-intermediate state (Belloni et al. 2002; Motta et al. 2011). The temporal analysis for the source XTE J1859+226 shows weak signature of QPOs in the PDS, during this phase of branch EF for the days from 63rd to 85th of the outburst as shown in Figure 4 (see also Casella et al. 2004). From Table 1, where we have summarized the details of temporal features during this phase, it can be observed that there is an evolution of QPO frequencies which initially increases from 8.42 Hz to 9.75 Hz (the total PDS rms increases from 4% to 5%) and then decreases to 4.62 Hz (total rms reduces to 2.7%). This evolution of QPO could be possibly similar to that observed during the primary outburst. Although the Q-factor is less, which can be due to decrease in flux as the source is in the declining phase of the outburst, all the QPOs observed can be classified as type C (see also Casella et al. 2004). Both the spectral and temporal properties seem to suggest that this phase/feature could be associated with a ‘secondary’ emission, within the same outburst.

As the source approaches the end phase of branch EF, there is a sudden increase in the photon index from 2.2 to 3.2 (spectral data fitted upto 15 keV), but with large errors (star points in Figure 8). This turns out to be a puzzling nature, as the disk temperature is reducing implying the low/hard state in the declining phase of the outburst.

It is observed that during the branches CD and EF, we observe the presence of QPOs of types A, B, a few C and C* (see

Table 1. Details of temporal characteristics during the ‘secondary’ outburst

MJD	Day	QPO frequency (Hz)	Significance of QPO	QPO rms (%)	Q-factor
51522.944	62.18	0	0	0	0
51523.941	63.18	8.42	1.36	6.46	2.54
51524.940	64.18	8.66	2.04	6.87	3.02
51525.353	64.59	8.21	2.48	6.03	4.02
51527.004	66.24	9.18	3.75	8.02	9.24
51527.736	66.97	9.75	2.56	8.03	3.23
51530.133	69.37	8.64	2.66	6.32	3.11
51546.036	85.27	4.62	2.90	3.82	4.58
51547.766	87.00	0	0	0	0

Casella et al. 2004). In Figure 11, we show the variation of disk and powerlaw flux as a function of QPO frequency. We observe that during the rising phase (hard and hard-intermediate states) the QPO frequency of type-C increases as both the disk and powerlaw flux increases, implying a positive correlation. During the soft-intermediate state (branch CD) the type B QPOs are observed to be correlated with the the powerlaw (non-thermal) flux but not with the disk flux. A few type C QPOs observed during the soft-intermediate state (branch CD) are observed not to show any correlation with the powerlaw flux. This variation is not similar to that observed for GX 339–4 by Motta et al. 2011, where both type B and C QPOs are correlated with the disk and powerlaw flux (see Figures 5 and 8 in Motta et al. 2011). Figure 11 also shows that the type C* QPOs do not have any correlation with the disk flux and powerlaw flux, while a correlation was observed with powerlaw flux for GX 339–4 by Motta et al. 2011. Type A QPOs do not show any correlation with flux for GX 339–4, while XTE J1859+226 has only very few type A QPOs, which limits the results.

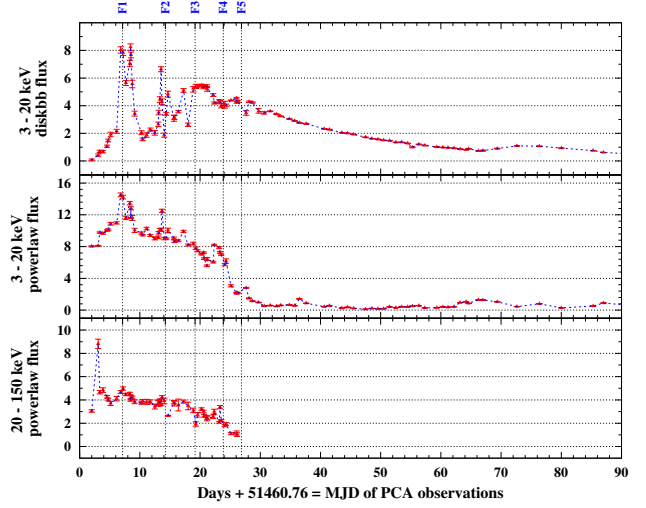
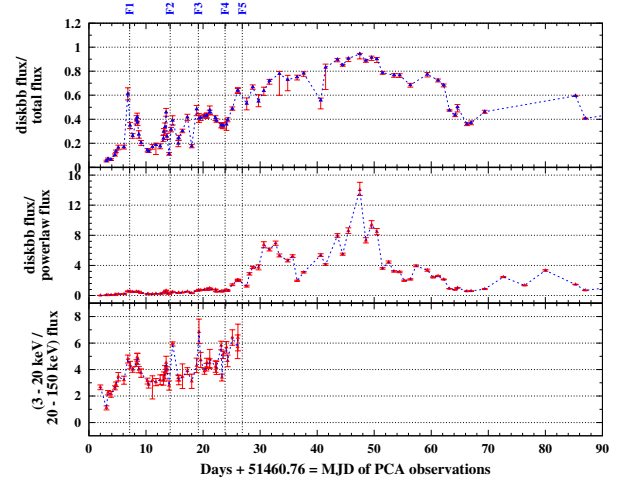
Sobczak et al. 2000 and McClintock et al. 2009 observed a positive correlation between QPO frequency and disk flux during the rising phase (for GRO J1655–40, XTE J1550–564, H 1743–322), which is also observed for XTE J1859+226. An opposite correlation was observed between QPO frequency and powerlaw flux for GRO J1655–40, while a positive correlation was observed for XTE J1550–564 and H1743–322.

3.1.6 Hard-intermediate state (branch FG)

In branch FG, we do not observe any QPOs and the power spectra remains to have broadband noise with total amplitude (rms) varying from 7% to 11%. The source is in the declining phase and it is observed from Figure 8 that the photon index reduces to 2.0. The spectra is dominated by powerlaw component, although we find weak signature of thermal flux with reduced inner disk temperature. The disk and powerlaw flux are observed to decrease without any signature of hard X-ray spectral component.

3.1.7 Hard state (branch GH)

At the end of the outburst, the source finally moved towards the hard state, which has similar characteristics of that during the initial phase of the outburst. The amplitude (rms) of the power spectra has increased to ~25% without any signature of QPOs. The energy spectra are mostly powerlaw in nature with photon index around 1.4 without any signature of hard X-ray spectral component. Only the last three observations show a photon index of ≥ 2.1 although the source count rates are very less with large errors, and it was

**Figure 9.** Variation of the flux contribution by the disk component and powerlaw component in the energy range of 3 - 20 keV, and 20 - 150 keV powerlaw flux. Flux values are quoted in units of 10^{-9} ergs cm^{-2} s^{-1} .**Figure 10.** Variation of the fraction of disk flux over the total flux, fraction of disk flux over powerlaw flux in the energy range of 3 - 20 keV, and of the ratio in 3 - 20 keV to 20 - 150 keV flux. Flux values are quoted in units of 10^{-9} ergs cm^{-2} s^{-1} .

difficult to fit the spectra. The disk contribution becomes almost negligible during this state at the end of the outburst.

3.2 ‘Spectro-temporal’ signatures of the source during the flares

In this section, we present the results based on the variations of temporal and spectral features during radio flares i.e., when the jet ejections have taken place to understand the disk-jet symbiosis. In Table 2, we summarize the properties of the source during the flares. As mentioned in §2, we have performed an energy dependent study of the PDS (in the bands 2 - 6 keV, 6 - 13 keV and 13 - 25 keV) of all the observations, in order to understand the nature of the X-ray features during the flares.

Table 2. Details of X-ray properties (in 2-25 keV band) of the observations during all the flares

X-ray/Radio (ID/Flare)	X-ray Flux (cts/sec)	MJD	Date	Time	Radio flux (mJy)	QPO frequency (Hz)	QPO rms (%)	QPO significance	QPO type	Γ	T_{in} (keV)
40124-01-11-00 ^b	1505	51466.896	1999-10-15	21:30:08		5.9	15.4	6.83	C	2.35	0.88
40124-01-12-00	2714	51467.581	1999-10-16	13:57:20 (7 hrs) ^a		0	0	0	-	2.51	1.03
F1		51467.904	1999-10-16	21:41:45.6	114						
40124-01-13-00 ^c	2597	51467.961	1999-10-16	23:04:16		6.1	3.8	7.24	B	2.42	1.07
40124-01-23-01 ^b	1558	51473.890	1999-10-22	21:22:08		7.6	4.3	5.82	C*	2.22	0.87
40124-01-15-02	1726	51474.087	1999-10-23	02:06:40		0	0	0	-	2.25	0.97
40124-01-15-03	2045	51474.287	1999-10-23	06:54:40		0	0	0	-	2.32	1.00
40124-01-24-00 ^c	1984	51474.429	1999-10-23	10:18:08		5.8	2.7	7.36	B	2.44	1.04
40124-01-25-00	1248	51474.820	1999-10-23	19:41:20 (6 hrs) ^a		6.1	7.1	8.27	C	2.09	0.87
F2		51475.0	1999-10-24	00:00:00	19						
40124-01-31-00 ^b	1262	51478.777	1999-10-27	18:39:28		7.2	6.4	5.76	C*	2.16	0.94
40124-01-32-00	1637	51479.635	1999-10-28	15:15:28 (7 hrs) ^a		0	0	0	-	2.24	0.96
F3		51479.940	1999-10-28	22:45:07.2	31						
40124-01-33-01	1625	51480.044	1999-10-29	01:04:32		0	0	0	-	2.28	0.96
40124-01-36-00 ^c	1474	51483.106	1999-11-01	02:33:20		4.8	4.7	16.6	B	2.32	0.98
40124-01-37-02 ^b	1391	51484.275	1999-11-02	06:37:20 (8 hrs) ^a		4.4	3.3	10.6	B	2.25	0.94
F4		51484.625	1999-11-02	15:00:35.8	5.2						
40124-01-38-00 ^b	1266	51484.872	1999-11-02	20:56:16		0	0	0	-	2.21	0.92
40124-01-39-00 ^c	952	51485.874	1999-11-03	20:59:44		6.9	3	5.56	C* ^e	2.14	0.87
40124-01-41-00 ^b	870	51487.009	1999-11-05	00:13:36 (15 hrs) ^a		4.7	2.1	7.59	C* ^e	2.34	0.85
F5^d		51487.635	1999-11-05	15:15:23.1	-						
40124-01-42-00	857	51488.41	1999-11-06	09:49:36		0	0	0	-	2.33	0.84
40124-01-49-00	502	51496.462	1999-11-14	11:06:24		0	0	0	-	2.10	0.79
40124-01-49-01 ^{c,b}	571	51497.254	1999-11-15	06:06:40		5.02	2.7	6.32	C* ^e	2.18	0.79
40124-01-50-01	502	51498.390	1999-11-16	09:22:24 (16 hrs) ^a		0	0	0	-	1.96	0.77
F6 (?)		51499.100	1999-11-17	02:24:00.0	7.9						
40124-01-51-00	406	51501.384	1999-11-19	09:13:36		0	0	0	-	1.90	0.76

Absence of QPO during F1 (in 2 - 5 keV and 13 - 25 keV band), whereas QPOs were absent in 2 - 25 keV during all other flares. ^a - minimum duration of X-ray observation before flare; ^b - observation of last QPO before flare; ^c - observation when QPO reappeared; ^d - No Radio observations, flare day based on ASM light curve (Brocksopp et al. 2002); ^e - Not classified in Casella et al. 2004

3.2.1 FLARE - I (F1)

The X-ray observation ~ 24 hrs before (MJD 51466.896) the radio flare peak on MJD 51467.9, shows the presence of a type C QPO of 5.97 Hz. The evolution of power spectra in soft (2 - 5 keV) and hard (13 - 25 keV) bands does not show any signature of QPO for the next observation (MJD 51467.581) which is 7 hrs before the flare peak. A broad 7.79 Hz type A QPO is observed, only above 5 keV as evident in the 6 - 13 keV PDS with rms amplitude of 3, which is typical for type A QPOs (Casella et al. 2004). So, in the overall

range of 2 - 25 keV, a broad QPO is observed. The next observation which is 2 hrs after the flare peak, shows a type B QPO of 6.1 Hz in all the energy bands. We also observe that the total rms of the PDS reduces (see also Fender et al. 2009) to a value of 2.7 when the QPO is not observed. Figure 12 shows the variation in the PDS for the energy range of 2 - 5 keV, for observations before and after the flare peak, implying the absence of QPO.

It is seen that, before the flare occurred i.e., when the QPO was present, the hard photons slightly lag behind the soft photons.

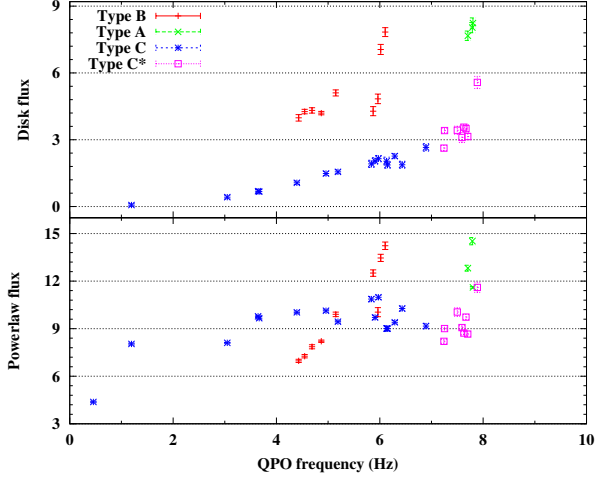


Figure 11. Variation of the disk flux and powerlaw flux with increase in QPO frequency. The flux values are quoted in units of 10^{-9} ergs cm^{-2} s^{-1} .

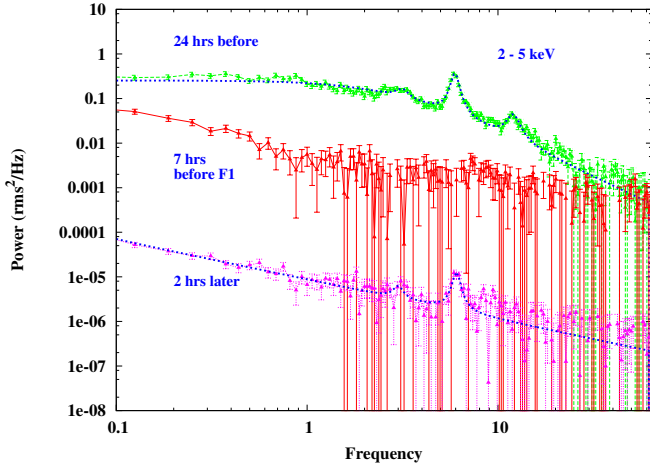


Figure 12. Variation of the PDS implying the absence of QPO in the energy range of 2 - 5 keV, during the first flare (F1). The power shown in y-axis has been scaled by a factor of 100, 1 and 0.1, from the top to bottom.

7 hrs before the flare peak, the 2 - 5 keV soft photons are lagging compared to 5 - 25 keV hard photons. When the QPO is observed again in the PDS, the hard photons are observed to lag.

We also note that before the flare peak, the photon index increased to 2.51, disk temperature increased from 0.88 keV to 1.06 keV (Table 2 and Figure 6) and the fold energy of the electrons increased from 151 keV to 201 keV. The disk flux increased from 2.14×10^{-9} ergs cm^{-2} s^{-1} to 8.03×10^{-9} ergs cm^{-2} s^{-1} (Figure 9) and dominated over the powerlaw flux (3 - 20 keV) by a factor of 0.55. The 3 - 20 keV flux is found to be more than the 20 - 150 keV flux, by a factor of 5 (Figure 10), suggesting the soft nature of the spectrum. This implies that the emission is disk dominated.

After the flare, the photon index decreased to 2.42 and disk flux reduced to 7.83×10^{-9} ergs cm^{-2} s^{-1} . This implies the hard nature of the spectrum although the disk temperature was around 1.07 keV and the fold energy had reduced to 156 keV.

Due to lack of X-ray observations during the flare and just before/after, we could not see a complete absence of the QPO in 2 - 25 keV band. Hence the broad QPO seen just 7 hrs before the

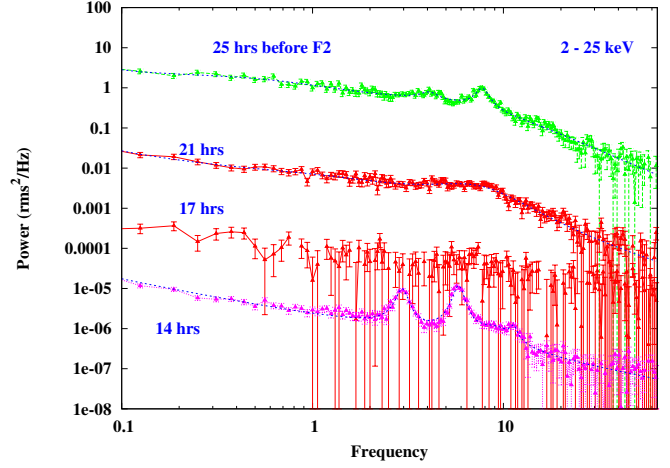


Figure 13. Evolution of the PDS in the energy range of 2 - 25 keV during the 2nd flare (F2). Absence of QPO is seen ~ 17 hrs before the radio flare peak of F2. The power spectra are scaled by factor of 1000, 10, 1, 0.01 from top to bottom.

flare peak, in the 6 - 13 keV band, suggests a partial vanishing of the QPO (See also Markwardt 2001). The spectrum also partially softens as compared to the spectrum of the observation before the flare.

3.2.2 FLARE - II (F2)

Radio observation shows that the flare F2, peaked on MJD 51475.0 with a flux of 19 mJy. 25 hrs earlier (MJD 51473.89) to the peak of F2, we observe type C* QPOs in the PDS. The observations ~ 21 hrs before (MJD 51474.087) peak of F2 shows a weak signature of QPO with an increase in frequency but of decreasing power. 4 hrs later (MJD 51474.287) the PDS of F2 shows complete absence of QPOs and the total rms reduces to 3.02 (see also Fender et al. 2009). *Cathedral B*-type QPOs are observed at frequencies 3 Hz & 6.1 Hz in the next X-ray observation which is 14 hrs before (MJD 51474.429) peak of F2. The evolution of power spectra is shown in Figure 13, which clearly indicates the ‘absence’ of QPO during the flare, but QPO reappeared before the flare peak (see §4 for discussion).

We find that when the QPO is not significant in the power spectra, the soft photons are lagging. 17 hrs before peak of flare F2 where there is a complete absence of QPO, no lag of soft to hard photons is seen. When the QPO is observed again, ~ 14 hrs before peak of F2, the hard photons are observed to lag behind the soft photons.

The corresponding softening of the spectra is also observed in the variation of the spectral parameters. When the QPO was not present (over MJD 51473.89 to MJD 51474.287), we noted that the disk temperature increases from 0.87 keV to 1 keV, and the photon index also increased from 2.22 to 2.32. The disk flux increased from 2×10^{-9} ergs cm^{-2} s^{-1} to 7×10^{-9} ergs cm^{-2} s^{-1} (Figure 9), but the fold energy increased from 83 keV to 138 keV. The ratio of disk flux over powerlaw flux increased from 0.43 to 0.65 with a significant decrease in hard X-ray flux (Figure 10). When the QPO was observed again, the photon index further increased to 2.44, with the disk temperature ~ 1 keV only. The disk flux reduced to $\sim 4.28 \times 10^{-9}$, whereas the fold energy increased to 154 keV. This suggest that, the nature of variation in spectral features

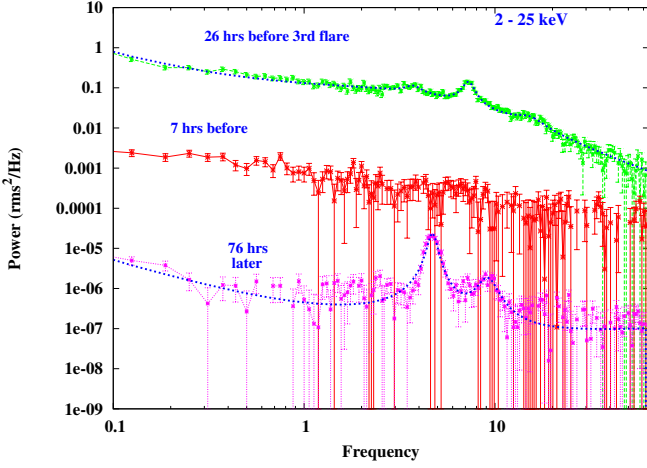


Figure 14. Evolution of the PDS in the energy range of 2 - 25 keV during the F3. QPOs are absent ~ 7 hrs before the radio flare peak of F3. The power spectra are scaled by factor of 100, 10, 0.01 from top to bottom.

along with the temporal properties (i.e., QPO features) during F2, is different from that of flare F1 and hence disk-jet symbiosis could be further complex (see §4 for discussions).

3.2.3 FLARE - III (F3)

On MJD 51478.777, a 7.2 Hz type C* QPO is observed. Radio observations indicate that multiple flares (see Figure 1) have occurred on MJD 51479.94 within ~ 40 hrs of gap with flux values of 31 mJy & 24 mJy during the period when F3 occurred. The X-ray observation which is around 7 hrs before F3, does not show any signature of QPO and the PDS is dominated by broad-band noise component (Figure 14). The subsequent X-ray observations does not show QPOs with decreased total rms (see also Fender et al. 2009) of 2.4. QPOs are observed almost after 3 days at a frequency of 4.8 Hz (type-B).

We find an indication of soft photon lagging just before the flare peak, whereas during the complete absence (~ 3 days) of QPO, no lag is observed. The hard photons are observed to be lagging, when the QPO is observed again after 3 days (see Figure 15).

During F3, disk temperature and photon index increases slightly, whereas the soft flux increased from 2.2×10^{-9} ergs $\text{cm}^{-2} \text{s}^{-1}$ to 5.2×10^{-9} ergs $\text{cm}^{-2} \text{s}^{-1}$ (Figure 9), which implies the softening of the spectra. The fold energy decreased from 126 keV to 97 keV. We also note that during the observations where there were no QPOs, disk flux dominates over the powerlaw flux by a factor of 0.6 to 0.9 with a significant decrease in hard X-ray flux (see bottom panel of Figure 10). At the same time, the powerlaw index and fold energy varies, but the disk temperature remains almost constant (Figure 6).

The QPOs observed before and after the ejections during the flares F1, F2 and F3 are of type C/C* and type B respectively (see Table 2).

3.2.4 FLARE - IV (F4)

Around 8 hrs before (i.e. on MJD 51484.27) the peak of next flare F4, a type B QPO is observed. The subsequent observations (on MJD 51484.87 and MJD 51485.07) does not show any signature of

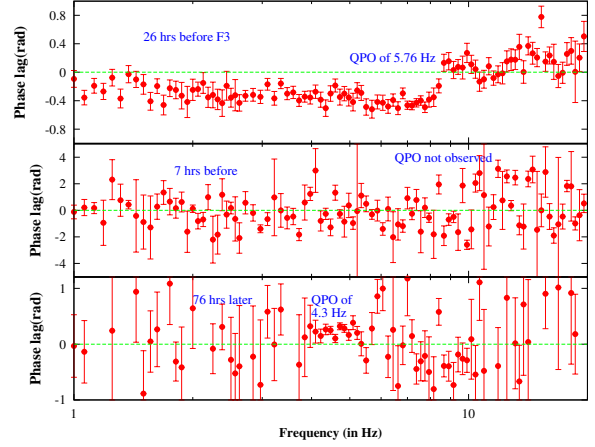


Figure 15. The variation in phase lag during the occurrence of flare F3. No phase lag is observed when QPO is not observed in the PDS.

QPOs (Figure 4), except broadband noise in the PDS (power spectra evolution not shown here) with decreased total rms of 2.5 which is consistent with Fender et al. 2009. It is also clear from Figure 1 that a flare has occurred with a flux of 5.2 mJy (MJD 51484.625). Brocksopp et al. 2002 reported the time of flare based on X-ray observation from ASM. 6 hrs after the peak of F4 (MJD 51484.87), QPOs are completely absent in the power spectra and are observed only after 30 hrs (on MJD 51485.874) at a frequency of 6.97 Hz (type C* with less rms and less Q-factor; see Casella et al. 2004 for details of type C* QPOs).

During the flare F4, soft photons are observed to be lagging, while in flares F2 and F3, no lag of soft to hard photons was observed.

It is also seen from Figure 6 and Table 2 that during the flare peak, the spectral index varies around 2.2. The disk temperature remained around 0.9 keV, whereas the fold energy varied around 150 keV (Figure 6). The ratio of low energy to high energy flux increases with a factor of ~ 6 (lower panel of Figure 10), implying the nature of spectral softening. The disk flux dominated over the non-thermal flux by a factor of 0.57 to 0.71, as seen in Figure 10. When the QPO was observed again, the photon index decreased to 2.14, with inner disk temperature of ~ 0.87 keV, and decreased fold energy of 96 keV.

3.2.5 FLARE - V (F5)

We observe a 4.7 Hz QPO in the PDS of MJD 51487.01. Although the Q-factor is less, these QPOs can be considered as of Type C* class based on the QPO frequency and amplitude. The next X-ray observation (MJD 51488.41) does not show a significant QPO in the PDS, with the total rms value reduced to 4 (see Figure 16). Brocksopp et al. 2002 has reported a ejection/jet (radio flare), to have occurred on MJD 51487.635, based on the X-ray observations by ASM (see also Fender et al. 2009). But there were no radio observations (see bottom panel of Figure 1) during this time. We suggest that, since (a significant QPO is not observed on the next observation of MJD 51488.41, the radio flare would have occurred on or before the time reported by Brocksopp et al. 2002. QPOs (type C*) are observed only after ~ 10 days (MJD 51497.25).

Thus during F5 we observe that the QPO observed before and after the flare is of type C*, whereas during flare F4 the evolution

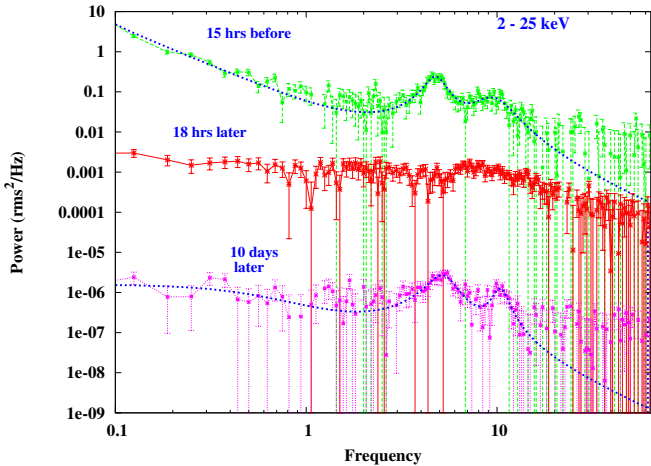


Figure 16. Evolution of the PDS in the energy range of 2 - 25 keV during F5. Scaling factors of 1000 is applied for the first PDS, 10 for the second and 0.01 is considered for the third.

of QPO is from type B to type C*. These features are not similar to that observed during the flares F1, F2 and F3.

The variation in spectral parameters does not show any significant change during the flare F5. The photon index is seen to vary in between 2.38 and 2.33, while the disk temperature remains almost constant around 0.79. Although the disk flux decreased from 4.24×10^{-9} ergs cm $^{-2}$ s $^{-1}$ to $\sim 3.48 \times 10^{-9}$ ergs cm $^{-2}$ s $^{-1}$, the ratio of disk to power-law flux is observed to increase by a factor of 3 to 6.7 (top panel of Figure 10) along with significant decrease of hard X-rays photons (beyond 50 keV), implying the softening nature of the spectrum. When the QPO is observed again, the photon index has reduced to 2.18 with the disk temperature of ~ 0.79 keV. The disk flux value is observed to dominate over the non-thermal flux, but with a lesser factor of 1.9.

We observe a signature of QPO (type C* with lesser Q-factor) at 5.02 Hz (on MJD 51497.25), after 10 days of flare F5. The next observation (on MJD 51498.39) does not show any QPOs (Figure 4) in the PDS, except a broad band noise. The total rms of the PDS reduces from 4.02 to 1.6. Radio observations also show that the flux decreases to ~ 1 mJy and later the source becomes non-detectable. We find that, there is a radio brightening (see Brocksopp et al. 2002) on MJD 51499.10 (after 16 hrs of X-ray obs.) of flux of 7.9 mJy (Figure 1), implying the possible signature of occurrence of a flare that could have triggered on or before this time.

4 DISCUSSIONS AND CONCLUDING REMARKS

The evolution of temporal and spectral properties of the source XTE J1859+226 during the 1999 outburst suggests that the source does evolve via different spectral states throughout the outburst. Detailed analysis during the multiple ejections (i.e., radio flares) reveals that the ejections are possibly associated with the inner part of the accretion disk, and hence the sudden ‘appearance’ of such radio flares or ‘jets’ could be because of some instability happening in the inner-part of the disk (i.e., ‘Comptonized’ corona). Although several attempts have been made to understand the evolution of ‘spectro-temporal’ characteristics as well as the ejection events observed in outbursting BH sources, till date, there is no comprehensive picture for the 1999 outburst of XTE J1859+226.

In this paper, we attempted to understand the possible ac-

cretion dynamics associated with the evolution of various X-ray features of XTE J1859+226, in the context of Two Component Advective Flow (TCAF) model (Chakrabarti & Titarchuk 1995; Giri & Chakrabarti 2013). According to TCAF, the Compton cloud (formed in shocked accretion phase) is nothing but the sub-Keplerian matter dominated CENTrifugal pressure supported BOundary Layer (i.e., CENBOL), which intercepts soft photons, mostly originated from the Keplerian disk, and the CENBOL up-scatter them via inverse Comptonization to produce high energy photons. The CENBOL surface may oscillate due to the oscillation of shock, which could be responsible for the generation of QPOs (Molteni et al. 1996; Ryu et al. 1997; Chakrabarti & Manickam 2000; Lee et al. 2011, see references therein). Again the oscillation of shock front in the disk depends on the physical properties of the sub-Keplerian flow (i.e., viscosity, angular momentum, energy etc.) and hence it could be possible to explain all types of QPOs in BH sources. Studies are in progress (SPH and TVD simulation) and will be presented elsewhere (Nandi et al., in prep.).

During the rising phase, we observe a monotonic increase of QPO frequency (C type) from 0.46 Hz to 6.09 Hz in both hard and hard-intermediate states. This happens because, the size of the region (i.e., the CENBOL), which is oscillating, is moving towards the hole and hence the QPO frequency increases (Chakrabarti et al. 2008, 2009; Nandi et al. 2012). We estimated the shock location (size of CENBOL) based on the POS solution (see §3.1). During this period, the instantaneous shock location (see Figure 5) and hence the ‘Compton cloud’ varies from $84.8 r_g$ to $21.2 r_g$. Using the same solution, we also estimated the size of the CENBOL region, before and after the flare.

During the soft-intermediate state, the QPO frequency (all types of QPOs) varies in between 6 Hz to 8 Hz, and this implies that the size of the inner part of the disk remains almost constant (i.e., shock location varies between $21.2 r_g$ to $17.7 r_g$). We also found that QPOs in the soft-intermediate state are sporadic in nature i.e. OFF (QPO not observed) and ON (QPO observed again), which could be linked with jet ejection (see Figure 4 and below for discussion). During the declining phase of soft-intermediate (except during the secondary emission of outburst), hard-intermediate and hard states, QPOs are hardly observable, whereas for other BH sources like GX 339–4, H1743–322, XTE J1550–564 QPOs are observed (Chakrabarti et al. 2009; Nandi et al. 2012; Debnath et al. 2013).

Titarchuk et al. 2007 evoked the idea of the diffusive propagation of perturbation in the disk like configuration of Keplerian (as extended disk) and sub-Keplerian (inner part of the disk as ‘Compton’ cloud) matter distribution (Chakrabarti & Titarchuk 1995), to understand the different noise component in the power spectra. So, the evolution of total rms as well as modeling the broadband power spectra of different branches of HID of XTE J1859+226 could also be possible to explain in the context of TCAF model, although detailed modeling of evolution of the power spectra of the source is beyond the scope of the present work.

The evolution of the HID (Figure 3) shows that during the rising phase, the source was initially in the hard state (region AB), and the variation of the spectral parameters, suggest that the spectra is mostly dominated by the sub-Keplerian component (i.e., larger ‘Compton’ cloud) with negligible contribution from the Keplerian disk. As the source moves towards the hard-intermediate state (implied by Figures 3 and 6), we observe that thermal flux increases relatively more than the non-thermal flux (Figure 9) and both are correlated with the increase in frequency of type C QPOs (see Figure 11). This implies that the Keplerian flow starts increasing along

with the sub-Keplerian flow, which is still dominating over the Keplerian in the hard-intermediate state (BC of HID). As a result, the spectra becomes softer and the size of the inner part of disk (i.e., CENBOL) also starts decreasing (see Figure 5). This is evident from the increase of QPO frequencies during the hard-intermediate state. It is observed that as the source move from hard to hard-intermediate states, the fold energy also (see Figure 7) increases. The increase in fold energy seems to be quite ‘unnatural’ compared to other BH sources, like GX 339–4 and XTE J1550–564, where Motta et al. 2009 and Titarchuk & Shaposhnikov 2010 respectively, pointed out the monotonic decrease of cutoff energy during the rising phase. It seems that the shock acceleration mechanism, which converts fraction of thermal electron to the non-thermal electron within the Compton cloud, becomes more important as the source evolves in this phase, and hence the fold energy increases although the source spectra becomes softer and softer. Similar kind of behaviour is observed in the hard and soft state spectrum of Cyg X–1, which has been modeled using shock acceleration mechanism in TCAF (Chakrabarti & Mandal 2006).

During the soft-intermediate state (CD & EF) the evolution pattern of HID is complex. We find that the photon index varies in between 2.5 to 2.1 and disk temperature varies around 0.9 keV, whereas variation of diskbb and power-law flux is not at all correlated (see Figure 9). This unnatural variation of flux occurs in short time-scales (few hrs to day scales). Also, the fold Energy varies randomly about an average value of 130 keV within 1σ error limits, whereas change in fold Energy during rising phase is well above the 2σ error limit. We observe all types of QPOs during this phase. The B-type QPO correlates with power-law flux whereas its variation is random with disk flux. C-type QPO does not show any specific correlation neither with power-law flux nor with the disk flux. This could be because that during this phase, multiple ejections have taken place, and they are directly associated with the disk dynamics.

So, it is possible that sub-Keplerian flow plays a major role (to generate various types of QPOs, relation between various types of QPOs with flux) compared to the Keplerian flow, as the inner disk (i.e., ‘hot’ Compton cloud) evolves faster (i.e., less viscous) than the Keplerian disk.

We could observe a short presence of a ‘soft state’ during branch DE for a few observations (see Figure 3) where the hardness ratio is of ~ 0.1 and total rms of PDS $\sim 1\%$ to 2% without any signature of QPO. During this phase, the Keplerian flow supposed to dominate over the sub-Keplerian flow to produce softest spectrum. As observed, the energy spectra is dominated by thermal emission (see Figure 10) but harder in nature (disk temperature also less) compare to the soft-intermediate state (see Figure 6 and 8). Hence, the observed state could not be a ‘canonical’ soft state. This could be possible due to enhancement of sub-Keplerian flow during this time that makes the spectra harder alongwith the strong presence of Keplerian flow (i.e., thermal emission). Also, the multiple ejections during the soft intermediate state restrict the disk to become Keplerian dominated flow as the ejections are coupled with the inner part of the disk, which is mostly sub-Keplerian in nature.

While the source continued in the soft-intermediate state (branch EF), there is an indication of weak X-ray flaring activity (secondary emission) of around 24 days with peak emission on 69th day of the outburst (see Figure 1). The monotonic increase in QPO frequencies (see Figure 4) and increase in other spectral parameters (Figure 8, 9 and Table 1; see also Dunn et al. 2011a), indicate that there could be sudden increase in Keplerian as well

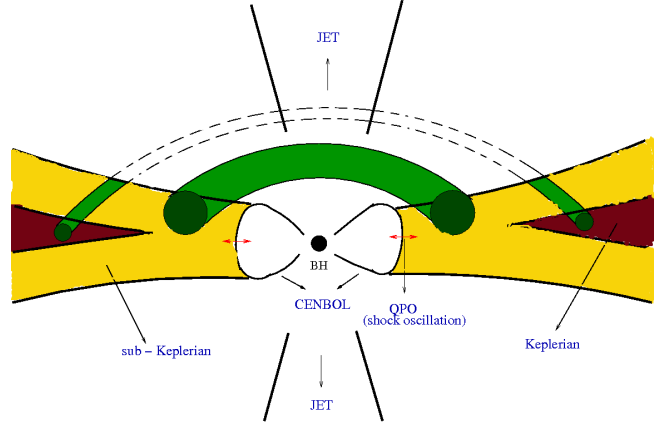


Figure 17. A pictorial representation of the magnetised-TCAF model, showing both the Keplerian and sub-Keplerian flows along with the toroidal magnetic flux tube and jet emission. (Adopted from Chakrabarti & Titarchuk 1995; Nandi et al. 2001). See Giri & Chakrabarti 2013 for simulation of TCAF model.

as in sub-Keplerian flow during the decline phase of the outburst, which results as a weak ‘secondary’ emission.

At the end of the outburst, the source transits from soft-intermediate to hard via hard-intermediate state before reaching the quiescence phase. The photon index starts decreasing, with a very weak signature of thermal emission (Figure 8 and 9), which implies that the emission component is again dominated by sub-Keplerian matter over Keplerian matter.

The modeling of the HID (i.e., q-track, see also Mandal & Chakrabarti 2010; Nandi et al. 2012) which follows the evolution of X-ray features of the outburst, and of the broadband spectrum (3 - 150 keV) will be carried out using TCAF model and will be presented elsewhere (Nandi et al. (in prep.)).

The sudden occurrence of a radio flare can be due to some disturbance in the disk system, which results in ejection of the material as jets. Several attempts have been made until now, to explain the phenomena of jet ejection in black hole binaries (see also Fender et al. 2009). Study of the jet emissions, using MHD simulations were carried out by Meier & Nakamura 2004, McKinney & Gammie et al. 2004 and De Villiers et al. 2005. These models suggests that the corona is like a windy hot material which blows away as jets from the inner regions of the accretion flow. In this work, we attempted to explain the ejection mechanism based on dynamics of magnetic flux tube inside the TCAF (see Figure 17) as described by Nandi et al. 2001.

When the ejection takes place due to the collapse of magnetic flux tube, the inner part of disk (i.e., CENBOL) gets disrupted and the matter is ejected as a jet. As a result, oscillation of the CENBOL (i.e., shocked surface) ceases and hence, there will not be any QPO in the PDS. The energy spectra are dominated by thermal emission from the disk, as the matter from the CENBOL (‘hot’ electron) is ejected. The fold energy is observed to increase just before the flare and decrease just after the flare. This could be the possible indication of ‘disruption’ of inner part of the disk. The subsequent ‘re-appearance’ (observation) of QPO and spectral hardening in a time scale of few hours to days suggest that the matter flows in sub-Keplerian disk forming the inner part of the disk (‘Compton’ cloud) responsible for QPO generation.

As the observation suggests that the companion is of K-type (Corral-Santana et al. 2011) and hence is magnetically active, it is

possible that the strong magnetic field anchored with the matter is continuously fed into the disk system during the rising phase of the outburst. Hence, during the transition from hard to soft-intermediate state, the field gets sheared and stronger (in the form of toroidal flux tube) and disrupts the inner part of the disk (in different time scale), resulting in multiple ejections at different time-scale.

For the flare F1, we observe a type C QPO of 5.97 Hz which corresponds to a CENBOL size of $21.2 r_g$. During the partial ‘disappearance’ (i.e., QPO is not observed in 2 - 5 keV band) of the inner part of the disk ~ 7 hrs before the flare peak, we observe a 7.79 Hz QPO at a shock location of $17.7 r_g$. Since the sub-Keplerian flow moves in shorter time scale it takes less duration of time to refill the inner part of disk to form the CENBOL again, which starts oscillating. Hence QPOs of 6.1 Hz (type B) are observed 2 hrs after the flare peak at a shock location of $20.8 r_g$. Thus, a duration of 9 hrs (maximum) was required for the CENBOL to get disrupted and refill.

During flare F2, a 7.7 Hz type C* QPO is observed at $17.9 r_g$ around 21 hrs before the flare peak. But within 7 hrs, the sub-Keplerian component (as the flow less viscous) has formed the corona and the oscillations of 5.87 Hz (type B) are re-stored at $21.4 r_g$. A closer look into the PDS evolution (Figure 13) shows that the QPO frequency increases with diminishing power, before the flare occurs and the QPO is not observed (see §3.2.4). Again the QPO re-appeared before the radio flare peak, which seems to be inconsistent as compare to other flares, where we observe a complete absence of QPO before the radio peak. We observe also similar characteristics in other sources like XTE J1550–564, where the time gap between QPO being not observed and the flare peak was more than 24 hrs (Radhika et al. (in prep.)). So, it is possible that the process of evacuation of the inner part of the disk is rather slow during F2, the ejected material took long time to peak as a radio flare. By that time, the inner part of the disk also started re-filling to form the corona to reproduce the QPO, which is interestingly of *Cathedral type*. As we mentioned, the QPO and Jet formation are coupled with the inner part of the disk, which is sub-Keplerian in nature. Hence, the disk-jet coupling mechanism in F2, which seems to be ‘complex’ in nature (‘spectro-temporal’ properties are totally different from other flares) could be due to the different dynamics (i.e., the amplification of magnetic field, motion of tube etc.) of flux tube within the CENBOL. It requires further investigation to study the coupling between flux tubes and sub-Keplerian flow and hence to understand the ‘complex’ disk-jet symbiosis. But, for both the flares F1 and F2, the disruption of the inner disk and refilling time is around 7 to 9 hrs. So, it is evident that within the hours time-scale only sub-Keplerian matter can easily move in, whereas Keplerian flow does not as it moves in viscous time-scale.

Before the peak of flare F3 a 7.24 Hz type C* QPO is observed corresponding to the CENBOL size of $18.6 r_g$. When the QPO is observed again at 4.87 Hz (type B) the shock location is $24.3 r_g$. We find that, the disruption and refilling time (presence of QPO) of the inner disk is ~ 3 days. It is possible that the magnetic field would have been strong enough (i.e., continuous collapse of flux tube) to disrupt the disk repeatedly, resulting in multiple signature of radio activity (see bottom panel of Figure 1). During this long disruption process, no lags in soft to hard photons are observed, disk temperature remains almost constant with increased disk flux and the fold energy decreases. These indicate that the ‘hot’ Compton cloud is ejected in the form of jets. As the source is also in the declining phase, the matter supply in both the form of Keplerian and sub-Keplerian flow has reduced and hence, took longer

duration to form the inner-part of the disk (i.e., CENBOL) for the oscillation to start again.

During F4, before the flare peak the QPO was observed at 4.43 Hz (type B) and the CENBOL size is of $25.9 r_g$. When the QPO is observed again its frequency is 6.97 Hz (type C*) at $19.1 r_g$. While before F5, the QPO observed is of 4.7 Hz (type C*) at $24.6 r_g$ and after the flare the QPO is again observed with frequency of 5.02 Hz (type C*) at $23.8 r_g$. The flares F4 and F5 occurred when the source was in the declining phase of the outburst, where the sub-Keplerian flow dominates. While in decay the rate of incoming matter (both the Keplerian and sub-Keplerian) from the companion reduces, and hence the strength of the magnetic field also reduces. So, we notice that the radio flares observed are with less peak flux as compared to previous flares although there is no radio observation during the flare F5 (See Brocksopp et al. 2002; Fender et al. 2009). As a result, during both the flares, the disruption and refilling time of inner part of the disk is longer of around 30 hrs for F4 (possibility of secondary emission after ~ 16.8 hrs with radio flux of ~ 8.9 mJy as shown in Figure 1) and 10 days for F5 respectively.

We found a possibility of occurrence of another radio flare (i.e., F6) on or before MJD 51499.10 with radio flux of ~ 7.9 mJy. There is an indication of QPO not being observed after the peak radio flux. As there is lack of X-ray and radio observations during this time, it is not possible to pinpoint the exact time of flare ejection.

Above discussions on all the flares suggests that the Radio flare takes different time to peak and QPO disappears during the flares. Re-appearance time scale (\sim few hrs to days based on available data) to produce QPO and hence the formation of ‘Compton’ cloud also suggests that the accretion flow could be sub-Keplerian in nature.

We observe that the type of QPO is independent of the ejection event (See §3.2 and Column 10 of Table 2). The results mentioned in §3.2 clearly shows that the QPOs observed before and after the flare, need not be of specific type. But, the prediction of Jet ejections (without any radio detection), based on QPOs disappear and reappear in power spectra, requires further studies in the context of TCAF model which could be possible after detailed investigation of X-ray observation of other outbursting sources.

We also have observed similar characteristics (no definite relation between the types of QPOs before and after the ejection) in other BH sources. In the case of XTE J1550–564, GRO J1655–40 and XTE J1752–223, we found that the QPO observed before and after the flare are of type C. For H1743–332, we observed a type C QPO before the ejection and the PDS showed a type B QPO after the ejection. So, in the present scenario, it is not possible to generalise or establish a relation between types of QPO and flare ejection events. Although, there were attempt to establish the link of B type QPOs with radio flare, along with the drop in rms in the power spectra (see Soleri et al. 2008; Fender et al. 2009). Detailed study on QPO types and radio flares will be performed for several BH sources (based on available X-ray and radio data) (Radhika et al. (in prep.)).

In the present work, we have not considered the type of QPOs before and after the ejections. It is quite possible to address the types of QPOs during the ejections, as the QPO generation in TCAF model depends on the sub-Keplerian flow characteristics (i.e., viscosity, angular momentum, energy etc. of the flow). This work is in progress which involves simulation (SPH and TVD based) and will be presented elsewhere.

There have been reports of flare events (radio ejections) during the outburst of sources like XTE J1748–288 (Brocksopp et al. 2007), XTE J1752–223 (Brocksopp et al. 2010) and H1743–322

(Miller-Jones et al. 2012). In the context of TCAF model, we will study the outburst evolution and flaring events associated with X-ray properties observed for the BH sources XTE J1748–288, XTE J1752–223, H1743–322, XTE J1550–564, GRO J1655–40, GX 339–4 and MAXI J1836–194. Preliminary results on the presence & absence of QPOs associated with flaring events for several outbursting black holes have been presented in Radhika et al. 2013; Nandi et al. 2013.

Finally, to summarize for the 1999 outburst of BH source XTE J1859+226:

- The source evolved through various states in HID with a sequence of *hard* → *hard-intermediate* → *soft-intermediate* → *soft state* (not ‘canonical’) → *soft-intermediate* → *hard-intermediate* → *hard states* before reaching to the quiescence phase. Multiple radio ejections (or the enhancement in sub-Keplerian flow) might have stopped the source to evolve from soft-intermediate to ‘canonical’ soft state.
- The QPO frequency increases monotonically during the rising phase of the outburst. The evolution is modelled with POS solution to estimate the size of the ‘Compton’ corona. Similar kind of variation is also observed in other outbursting BH sources.
- The temporal evolution of the PDS shows that the QPOs are not observed, during the ejection as observed in radio.
- During F1, no QPO is observed in the soft band of 2 - 5 keV, but a broad QPO of less amplitude is observed in the 6 - 13 keV band. This implies that there has been a partial absence of the QPO.
- During F2, F3, F4 and F5, we find that the QPOs are not at all observed in the PDS.
- The QPO frequency observed before and after the flare need not be of same type during all the flares.
- During all the ejections X-ray spectrum gets soften and fold energy (E_{fold}) decreases, as the inner disk (i.e., ‘hot’ electron cloud) gets disrupted and spectrum is dominated by disk emission. Only in the case of F2, E_{fold} increases since the evacuation process seems to be complex.
- ‘Disruption’ of inner part of the disk occurs as a resultant of dominant thermal emission over non-thermal flux and absence of QPOs. This could be due to the ‘catastrophic collapse’ of toroidal flux tube of strong magnetic field in the hot region of sub-Keplerian flow.
- During the declining phase, source might have undergone a secondary outburst observed as a weak X-ray flaring activity for ~ 24 days.
- Due to lack of continuous X-ray observation during the flare time, it was not possible to tighten the time duration of disruption and refilling time scale. So, it is required to have more precise and simultaneous observation in *radio-UV-X-rays* to provide better picture of disk-jet dynamics in outbursting sources. In this context, continuous monitoring of outbursting sources with India’s upcoming multi-wavelength satellite ASTROSAT (scheduled for 2014 launch) along with GMRT, VLBI etc. will be a best opportunity for studying the complex accretion dynamics of BH sources.

ACKNOWLEDGMENTS

We thank Dr. P. Sreekumar and Dr. S. Seetha of Space Astronomy Group, ISRO Satellite Centre (ISAC), Bangalore for various suggestions and support.

This research has made use of the data obtained through High Energy Astrophysics Science Archive Research Center on-line service, provided by NASA/Goddard Space Flight Center and of the

General High-energy Aperiodic Timing Software (GHATS) package developed by Dr. Tomaso Belloni at INAF - Osservatorio Astronomico di Brera.

We thank Dr. Dipankar Bhattacharya of Inter University Centre for Astronomy & Astrophysics, Pune for providing an opportunity to participate in the ‘Advanced X-ray timing workshop’ and also to Dr. Tomaso Belloni for the sessions on usage of GHATS.

REFERENCES

- Belloni T. M., Hasinger G., 1990, A&A, 230, 103
 Belloni T. M., Psaltis D., van der Klis M., 2002, ApJ, 572, 392
 Belloni T. M., Homan J., Casella P., et al., 2005, A&A, 440, 207
 Belloni T. M., Parolin I., Del Santo M., et al., 2006, MNRAS, 367, 1113
 Belloni T. M., 2010, ‘The Jet Paradigm - From Microquasars to Quasars’, Lect. Notes Phys 794, edited by T. Belloni, 794, 53
 Blandford R. D., Znajek R. L., 1997, MNRAS, 179
 Bradt H. V., Rothschild R. E., Swank J. H., 1993, A&A supplement series, 97, 355
 Brocksopp C., Fender R. P., McCollough M., et al., 2002, MNRAS, 331, 765
 Brocksopp C., Miller-Jones J. C. A., Fender R. P., Stappers B. W., 2007, MNRAS, 378, 1111
 Brocksopp C., Corbel S., Tzioumis T., Fender R., Coriat M., 2010, Atel, 2400
 Cadolle Bel M., Rodriguez J., D’Avanzo P. et al., 2011, A&A, 534, A119
 Casella P., Belloni T., Homan J., Stella L., 2004, A&A, 426, 587
 Casella P., Belloni T., Homan J., Stella L., 2005, ApJ, 629, 403
 Chakrabarti S. K., & D’Silva, S., 1994, ApJ, 424, 138
 Chakrabarti S. K., Titarchuk L. G., 1995, ApJ, 455, 623
 Chakrabarti S. K. & Manickam, S. G., 2000, ApJ, 531, L41
 Chakrabarti, S. K., Nandi, A., Manickam, S., Mandal, S. & Rao, A. R., 2002, ApJ, 579, L21
 Chakrabarti S. K., Acharya K., Molteni D., 2004, A&A, 421, 1
 Chakrabarti S. K., Mandal S., 2006, ApJ, 642, 49
 Chakrabarti S. K., Debnath D., Nandi A. & Pal P. S., 2008, A&A, 489, L41
 Chakrabarti S. K., Dutta B. G., & Pal P. S., 2009, MNRAS, 394, 1463
 Corral-Santana J. M., Casares J., Shahbaz T., Zurita C., Martinez-Pais I. G., Rodriguez-Gil, 2011, MNRAS, 413L, 15C
 De Villiers J. P., Hawley J. F., Krolik J. H., Hirose S., 2005, ApJ, 620, 878
 Debnath D., Chakrabarti S. K., Nandi A., 2008, BASI, 36, 151
 Debnath D. et al., 2013 submitted
 Dunn R. J. H., Fender R. P., Kording E. G., Belloni T., Cabanac C., 2011, MNRAS, 403, 61
 Dunn R. J. H., Fender R. P., Kording E. G., Belloni T., Merloni A., 2011, MNRAS, 411, 337
 Ebisawa, K. et al., 1994, PASJ, 46, 375
 Esin A. A., McClintock J. E., Narayan R., 1997, ApJ, 489, 865
 Fender R. P., Belloni T., Gallo E., 2004, MNRAS, 355, 1105
 Fender R. P., Homan J., Belloni T., 2009, MNRAS, 396, 1307
 Feroci M., Matt G., Pooley G., Costa E., Tavani E., Belloni T., 1999, A&A, 351, 985
 Garnavich P. M., Stanek K. Z., Berlind P., 1999, IAUC, 7276
 Gierlinski M., Done C., MNRAS, 347, 885
 Giri K., Chakrabarti S. K., 2013 MNRAS, in press
 Homan J., Belloni T., 2005 Ap&SS, 300, 107H

- Ingram A., Done C., 2011, MNRAS, 415, 2323
- Lee, S., Ryu, D., Chattopadhyay, I., 2011, ApJ, 728, 142
- Mandal S., Chakrabarti S. K., 2010, ApJ, 710, L147
- Markwardt C. B., 2001, Astrophysics & Space science, 276, 209
- McClintock J. E., Remilard R. A., 2006, 'Black hole binaries', Compact Stellar X-ray sources, edited by Lewin W. H. G. and M. van der Klis
- McClintock J. E., Remilard R. A., Rupen M. P., Torres M. A. P., Steeghs D., Levine A. M. et al., 2009, ApJ, 698, 1398
- McCollough M. L., Wilson C. A., 1999, IAUC, 7282
- McKinney J. C., Gammie C. F., 2004, ApJ, 611, 977
- Meier D. L., Nakamura M., Proceedings 3-D signatures in Stellar explosions, ed. P. Hoeflich, P. Kumar, C. Wheeler, 2004, Cambridge University press, 219
- Merloni A., Fabian A. C. and Ross R. R., 2000, MNRAS, 313, 193
- Meyer F., Liu B. F., Meyer-Hofmeister E., 2007, A&A, 463, 1
- Meyer-Hofmeister E., Liu B. F., Meyer F., 2009, A&A, 508, 329
- Miller-Jones J. C. A. et al., 2012, MNRAS, 421, 468
- Miyamoto S., Kimura K., Kitamoto S., Dotani T., Ebisawa K., 1991, ApJ, 383, 784
- Molteni D., Sponholz H., Chakrabarti S. K., 1996, ApJ, 457, 805
- Motta S., Belloni T., Homan J., 2009, MNRAS, 400, 1603M
- Motta S., Munoz-Darias T., Casella P., Belloni T., Homan J., 2011, MNRAS, 418, 2292
- Munoz-Darias T., Motta S. and Belloni T., 2010, MNRAS, 410, 679
- Nandi A., Chakrabarti S. K., Vadawale S. V., Rao A. R., 2001, A&A, 380, 245
- Nandi A., Debnath D., Mandal S., Chakrabarti S. K., 2012, A&A, 542, A56
- Nandi, A. & Radhika. D., 2012, COSPAR Scientific Assembly, Mysore, INDIA
- Nandi, A., Radhika. D. & Seetha. S., 2013, ASI Conference Proceedings (BASI), in press
- Nandi A. et al. (in prep.)
- Okuda T., Teresi V., Molteni D., 2007, MNRAS, 377, 1431
- Pooley G. G., Hjellming R. M., 1999, IAUC, 7278
- Radhika. D, Nandi A., and S. Seetha, 2013, Upcoming proceedings of the conference 'X-ray Astronomy : towards the next 50 years', Milan, ITALY (arXiv:1301.7234)
- Radhika. D et al. (in prep.)
- Remilard R. A. et al., 1999, ApJ, 552, 397
- Rodriguez J., Prat L., 2008, Proceedings of Science
- Rodriguez J., Varniere P., 2011 ApJ, 735, 79
- Ryu D., Chakrabarti S. K., Molteni D., 1997, ApJ, 474, 378
- Shakura N. I., Sunyaev R. A., 1973, A&A, 24, 337
- Sobczak G. J., McClintock J. E., Remilard R. A., Cui W., Levine A. M. et al., 2000, ApJ, 531, 537
- Soleri P., Belloni T., Casella P., 2008, MNRAS, 383, 10989
- Stiele H., Belloni T. M., Kalemci E., Motta S., 2013, MNRAS, 429, 2655
- Tagger M., Pellat R., 1999, A&A, 349, 1003
- Titarchuk L. G., 1994, ApJ, 434, 570
- Titarchuk L., Shaposhnikov N., & Arefiev V., 2007, ApJ, 660, 556
- Titarchuk L., Shaposhnikov N., 2010, ApJ, 724, 1147
- Titarchuk L., Osherovich V., 2000, ApJ, 542, L111
- Vadawale S. V., Rao A. R., Nandi A., Chakrabarti S. K., 2001, A&A, 370, L17
- Wagner R. M., Schmidt G. D., Shrader C. R., 1999, IAUC, 7279
- Wood A., Smith D. A., Marshall F. E., Swank J. H., 1999, IAUC, 7274
- Yang J., Brocksopp C., Corbel S., Paragi Z., Tzioumis T., Fender R. P., 2010, MNRAS, 409, L64
- Zhang W., Jahoda K., Swank J. H., Morgan E. H., Giles A. B., 1995, ApJ, 449, 930